

Electronic Supplementary Information

Novel Linear Oligoisoindole Compounds with Conjugated Electronic Structure

Yuehong Zhang, Chiming Wang, Xin Chen, Houhe Pan, Dongdong Qi,* Kang Wang,*
and Jianzhuang Jiang*

Caption of Content

1. NMR spectra section, pages S3-S4.
2. IR spectra section, page S5.
3. Simulated electronic absorption spectra section, pages S6-S7.
4. Experimental section, pages S8-S15;
5. Synthesis of linear oligoisoindole derivatives, Scheme S1, page S16;
6. Isotopic patterns and HR MS for **1-4**, Fig. S1-S4, pages S17-S20;
7. NMR spectra for **1-4**, Fig. S5-S15, pages S21-S31;
8. X-ray crystal structures of **1** and **4**, Fig. S16-17, pages S32-33;
9. Differential pulse voltammograms for **1-4**, Fig. S18, page S34;
10. Simulated absorption spectra for **1-4**, Fig. S19-S22, pages S35-S38;
11. The π bond order of cyclic oligoisoindoles and the phthalocyanine ring-cleavage derivative, Fig. S23, page S39;
12. IR spectra for **1-3**, Fig. S24, page S40;
13. Tautomeric conformations for **1-4**, Fig. S25, page S41;
14. ^{13}C NMR spectra for **1-3**, Fig. S26-S28, pages S42-S44;
15. The π MBO of **1-4**, cyclic oligoisoindoles, and the phthalocyanine ring-cleavage derivative, Fig. S29-S30, pages S45-S46;
16. X-ray crystal structure of **3**, Fig. S31, page S47;
17. MS, NMR and IR spectra for **5**, Fig. S32-S35, pages S48-S51;
18. NMR data for **1-4**, Table S1, page S52;
19. Crystallographic data for **1**, **3**, **4**, and **5**, Table S2, page S53;
20. Electron density difference plots of electron transitions for **1-4**, Tables S3-S6, pages S54-S57.

NMR spectra. As shown in Fig. S5, the ^1H NMR spectrum of **1** exhibits two singlets at $\delta = 7.77$ and 6.42 ppm due to the isoindole α protons. The signals for the aromatic protons of 2,6-diisopropylphenoxy substituents exhibited several multiplets in the range of $\delta 7.27$ - 7.23 ppm. The multiplets observed at $\delta 3.16$ - 3.13 ppm were attributed to the methyne protons on the 2,6-diisopropylphenoxy groups. The signals for the methyl protons on the 2,6-diisopropylphenoxy groups and protons on the $\text{SC}_{12}\text{H}_{25}$ chains are partially overlapped, leading to the observation of the multiplet in the range of $\delta 1.25$ - 1.06 ppm and two triplets at $\delta = 2.81$ and 0.85 ppm, respectively. As for **2**, Fig. S6 its ^1H NMR spectrum exhibits one broad signal at $\delta = 9.84$ ppm due to the isoindole N-H proton. The signals for isoindole α protons exhibited five singlets at $\delta = 7.92$, 6.85 , 6.67 , 6.59 , and 6.44 ppm, respectively, and were partially overlapped by the signals for the aromatic protons of 2,6-diisopropylphenoxy substituents which exhibited several multiplets in the range of $\delta 7.41$ - 7.23 ppm. The multiplet observed in the range of $\delta 3.16$ - 3.10 ppm is attributed to the methyne protons on the 2,6-diisopropylphenoxy groups. The signals for the methyl protons on the 2,6-diisopropylphenoxy groups and protons on the $\text{SC}_{12}\text{H}_{25}$ side chain are partially overlapped, leading to the observation of the multiplet in the range of $\delta 1.25$ - 1.06 ppm and two triplets at $\delta = 2.70$ and 0.85 ppm, respectively. Similar to that of **3**, the singlet at $\delta = 4.05$ ppm with the integral of two is assigned to the protons from one of the outer isoindole. As shown in Fig. S7, the ^1H NMR spectrum of compound **4** exhibits two broad signals at $\delta = 10.03$ and 8.85 ppm due to the isoindole N-H protons. The signals for the isoindole α protons were observed at $\delta = 7.52$ and 6.74 ppm and partially overlapped with the signals of the aromatic protons on the 2,6-diisopropylphenoxy substituents appearing at $\delta 7.42$ - 7.19 , 6.92 , 6.62 - 6.57 and 6.31 ppm. The multiplets in the range of $\delta 3.47$ - 2.98 and 1.33 - 0.72 ppm are attributed to the methyne and methyl protons of 2,6-diisopropylphenoxy substituents,

respectively. Similar to those of **2** and **3**, the singlet at $\delta = 4.17$ ppm is assigned to the protons from the sp^2/sp^3 terminal carbon atoms. The above mentioned assignment was further confirmed by the ^1H - ^1H COSY spectroscopic results of these compounds, Fig. S9-S13. Similar to compound **3**, there is also tautomerization of the N-H protons between the outer and inner isoindole units in compounds **2** and **4**, as shown in Fig. S11, S13, and S15. However, owing to the quite close energy between tautomer A and B in compound **2**, the coupling signals between the N-H protons from the isoindole units and the protons from the sp^2/sp^3 terminal carbon atoms could not be observed in the ^1H - ^1H COSY spectrum even at the temperature as low as 233 K.

IR spectra. The IR spectra of **1-3** were shown in Fig. S24. In addition to the bands associated with the oligoisoindole skeletons for **1-3** such as the C-H wagging and torsion vibrations (*ca.* 770 and 729 cm^{-1}), and the isoindole ring stretching vibrations (*ca.* 1445 and 1385 cm^{-1}),¹ the bands observed at *ca.* 2962, 2927, and 2868 cm^{-1} are assigned to the asymmetric and symmetric C-H stretching vibrations of the $-\text{CH}_3$ groups, while those at 1255 and 1046 cm^{-1} are ascribed to the asymmetric and symmetric C-O-C stretching vibrations of the 2,6-diisopropylphenoxy groups.² For **1** and **2**, a medium band at 2851 cm^{-1} is also found, due to the symmetric C-H stretching vibration of the methylene groups from the $\text{SC}_{12}\text{H}_{25}$ side chain(s).³

Simulated Electronic Absorption Spectra. As easily expected,⁴ despite the slightly overestimated transition energies, the simulated spectra for **1-4** are in good agreement with the experimental ones, Fig. S19-S22. As exemplified by compound **1** shown in Fig. S19 and Table S3, the intense absorptions in the region from 375 to 525 nm mainly originate from the transitions from HOMO/HOMO-4 to LUMO, involving electron density moving from the peripheral substituents to the conjugated diisoindole core together with the electron density rearrangement within the diisoindole core. While the weak absorption from 300 to 375 nm is associated with the electron transition from HOMO-2 to LUMO+1, mainly involving electron density transfer from peripheral substituents to the inner diisoindole core. The nature of the strong absorption from 250 to 300 nm is complicated, which is formed by coupling of absorptions mainly associated with the electron transitions from HOMO-2 to LUMO+3/LUMO+7 and HOMO-1 to LUMO+4/LUMO+8, involving electron density moving from the diisoindole core to the peripheral substituents. For compound **2**, Fig. S20 and Table S4, the intense absorption in the region from 375 to 550 nm mainly originates from the transitions from HOMO/HOMO-1 to LUMO, involving electron density moving from the peripheral substituents and conjugated core of the two C-C linked isoindole moieties (that do not contain the sp³ hybridized carbon atom) to the conjugated triisoindole core. The weak absorption from 300 to 375 nm is formed by coupling of absorptions mainly associated with the electron transitions from HOMO-3/HOMO-5/HOMO-6/HOMO-7/HOMO-9 to LUMO and HOMO to LUMO+1/LUMO+2, involving electron density moving from the peripheral substituents to the conjugated trisoindole core together with the electron density rearrangement within the trisoindole core. This is also true for the strong absorption in the range from 250 to 300 nm, formed by coupling of absorptions mainly associated with the electron transitions from HOMO to LUMO+8/LUMO+9, HOMO-1 to LUMO+4/LUMO+11/LUMO+14, and HOMO-2 to LUMO+2/LUMO+9, involving

electron density moving from the peripheral substituents and conjugated core of the two isoindoles linked by C-C bond to the peripheral substituents. This is also true for compound **3** and **4**, Fig. S21 and S22, and Tables S5 and S6.

Experimental Section

General Remarks: Column chromatography was carried out on silica gel (Merck, Kieselgel 60, 70-230 mesh) column with the indicated eluents. All other reagents and solvents were used as received. 4,5-Bis(2,6-diisopropylphenoxy)phthalonitrile⁵ was prepared according to the published procedure. NMR spectra were recorded on a Bruker DPX 400 spectrometer. Spectra were referenced internally using the residual solvent resonances relative to SiMe₄. Electronic absorption spectra were recorded on a Lambda 750 spectrophotometer. Fluorescence spectra were recorded on an F4500 (Hitachi) with the excitation wavelength of 510 nm and Rhodamine B was employed as the reference compound to obtain the fluorescence quantum yields. IR spectra were recorded as KBr pellets using a Bruker Tensor 37 spectrometer with 2 cm⁻¹ resolution. HR (high resolution) MALDI-TOF mass spectra were recorded on Solarix FT-ICR-MS with *dithranol* as the matrix. Electrochemical measurements were carried out with a BAS CV-50W voltammetric analyzer. The cell comprised inlets for a glassy-carbon-disk working electrode with a diameter of 2.0 mm in diameter and a silver-ware counter electrode. The reference electrode was Ag⁺/Ag (a solution of 0.01 M AgNO₃ and 0.1 M TBAP in acetonitrile), which was connected to the solution by a Luggin capillary whose tip was placed close to the working electrode. It was corrected for junction potentials by being referenced internally to the ferrocenium/ferrocene (Fc⁺/Fc) couple [$E_{1/2}(\text{Fc}^+/\text{Fc}) = 0.501 \text{ V vs. SCE}$]. Typically, a 0.1 M solution of [NBu₄][ClO₄] in CH₂Cl₂ containing 1 mM of sample was purged with nitrogen for 10 min, and then the voltammograms were recorded at ambient temperature. The scan rate was 20 mV/s for the electrochemical measurement.

X-ray crystallographic analysis of 1, 3, 4 and 5. Single crystals of **1**, **3**, **4** and **5** suitable for X-ray diffraction analysis were obtained by slow diffusion of methanol into the toluene, CHCl₃, CH₂Cl₂ and CHCl₃ solution of respective compound, respectively. The

linear diisindole **1** crystallizes in the triclinic space group *P1* with one molecule per unit cell, while the tetraisindole **3** crystallizes in the monoclinic space group *P21/c* with two molecules per unit cell, the hexaisindole **4** crystallizes in the triclinic space group *P-1* with two molecules per unit cell, and the tetraisindole **5** crystallizes in the triclinic space group *P-1* with one molecule per unit cell. The corresponding crystallographic and structural data are summarized in Table S2. Data were collected on an Oxford Diffraction Gemini E system with Cu_{Kα} radiation $\lambda = 1.5418 \text{ \AA}$ at 150 K, using a ω scan mode with an increment of 1°. Preliminary unit cell parameters were obtained from 30 frames. Final unit cell parameters were obtained by global refinements of reflections obtained from integration of all the frame data. The collected frames were integrated using the preliminary cell-orientation matrix. The SMART software was used for data collecting and processing; ABSpack for absorption correction;⁶ and SHELXL for space group and structure determination, refinements, graphics, and structure reporting.⁷ CCDC-1510099, 1542987, 1546494, and 1550842 contain the supplementary crystallographic data for this paper. These data can be obtained free of charge from the Cambridge Crystallographic Data Centre via www.ccdc.cam.ac.uk/data_request/cif.

Density functional theory (DFT) and time-dependent density functional theory (TD-DFT) together with Mayer bond order (MBO) analysis. The DFT method was used to calculate the electronic structures of **1-4** and the corresponding Mayer bond order, and the TD-DFT method was used to simulate the electronic absorption spectra of **1-4**. In all the cases, the functional and basis set of τ HCTHhyb/6-31G(d) was employed. The probabilities of the tautomers are calculated on the basis below: If one molecule has *N*

tautomers, the ratio of *n*th tautomer can be calculated using

$$Ratio(n) = \frac{e^{-\frac{E_n}{kT}}}{\sum_{i=1}^N e^{-\frac{E_i}{kT}}}, \text{ where } E_n$$

is the energy of the n th isomer, k is the Boltzmann constant, and T is the temperature. All the calculations were carried out by using the Gaussian 09 (Revision D.01) program.⁸

The Mayer bond order (MBO)⁹ between Atom A and Atom B is defined in the following manner:

$$BO_{AB} = BO_{AB}^{\alpha} + BO_{AB}^{\beta} = 2 \sum_{a \in A} \sum_{b \in B} [(P^{\alpha}S)_{ba}(P^{\alpha}S)_{ab} + (P^{\beta}S)_{ba}(P^{\beta}S)_{ab}]$$

where P^{α} and P^{β} is the α -spin and β -spin density matrix, respectively; S is the overlap matrix between Orbital a and Orbital b defined as $S = \int \varphi_a(\vec{r})\varphi_b(\vec{r})d\vec{r}$.

When the σ electrons are deleted in the wave function, the π -MBO¹⁰ will be calculated out to clarify the π bonding nature. The choice of σ/π electrons can be controlled by the coefficient of basis functions:

$$\pi BO_{AB} = \pi BO_{AB}^{\alpha} + \pi BO_{AB}^{\beta} = 2 \sum_{a \in A} \sum_{b \in B} [(P^{\alpha}S_{\pi})_{ba}(P^{\alpha}S_{\pi})_{ab} + (P^{\beta}S_{\pi})_{ba}(P^{\beta}S_{\pi})_{ab}]$$

$$S_{\pi} = \int \varphi_{\pi a}(\vec{r})\varphi_{\pi b}(\vec{r})d\vec{r}$$

$$\varphi_i(\vec{r}) = \varphi_{\pi i}(\vec{r}) + \varphi_{\sigma i}(\vec{r})$$

$$\begin{cases} \varphi_{\pi i}(\vec{r}) = \mu_i \sum_l \gamma_{\pi} C_{l,i} \chi_l(\vec{r}) : \begin{cases} \text{if } \chi_l(\vec{r}) \text{ is pure } \pi \text{ type, } \gamma_{\pi} = 1 \\ \text{if } \chi_l(\vec{r}) \text{ is pure } \sigma \text{ type, } \gamma_{\pi} = 0 \end{cases} \\ \varphi_{\sigma i}(\vec{r}) = \mu_i \sum_l \gamma_{\sigma} C_{l,i} \chi_l(\vec{r}) : \begin{cases} \text{if } \chi_l(\vec{r}) \text{ is pure } \pi \text{ type, } \gamma_{\sigma} = 0 \\ \text{if } \chi_l(\vec{r}) \text{ is pure } \sigma \text{ type, } \gamma_{\sigma} = 1 \end{cases} \end{cases}$$

where $\varphi_{\pi i}(\vec{r})$ and $\varphi_{\sigma i}(\vec{r})$ are the modified wave function of orbital i , which only describes the π and σ orbitals, respectively; μ_i is the occupying number of the i th orbital; $\chi_l(\vec{r})$ is the l th basis function in the i th orbital; γ_{σ} and γ_{π} is the signal of $\chi_l(\vec{r})$ type; $C_{l,i}$ is the element of l th row and j th column in the expansion coefficient matrix.

It is worth noting that the judgment of σ/π type of the basis function $\chi_l(\vec{r})$ is the key point in the calculation of π -MBO. When the Pople basis set is employed, the judgment is based on the mathematical expression of the given basis function.

1) If the mathematical expression is *s*-type, for example $\chi_s(v, \vec{r}) = \left(\frac{2v}{\pi}\right)^{\frac{3}{4}} e^{-\alpha \vec{r}^2}$,¹¹

this basis function should be a pure σ -type. Here, γ_σ is 1 while γ_π is 0.

2) If the mathematical expression is *p*-type, for example

$\chi_{p_x}(v, \vec{r}) = \left(\frac{128v^5}{\pi^3}\right)^{\frac{1}{4}} x e^{-\alpha \vec{r}^2}$,¹¹ this condition should be divided into three cases:

2.1) If this basis function is symmetric relative to the given conjugated plane (in other word, this basis function should be parallel to the given conjugated plane), it should be a pure σ -type function. Here, γ_σ is 1 while γ_π is 0.

2.2) If this basis function is anti-symmetric relative to the given conjugated plane (in other word, this basis function should be vertical to the given conjugated plane), it should be a pure σ -type function. Here, γ_σ is 1 while γ_π is 0.

2.3) If this basis function is neither parallel nor vertical, but sloping to the given conjugated plane, it should be considered as a contributor to both σ -bonding and π -bonding. If θ is set to describe the angle between this basis function and the given conjugated plane, γ_σ will be expressed as $\cos(\theta)$ meanwhile γ_π as $\sin(\theta)$.

In the present work, the N-H tautomerization is a special difficulty in the bond order analyses. For example, there are 3 isomers for **3**, Fig. S25. The average π -MBO can be expressed as

$$\overline{\pi BO}_{AB} = \sum_{n=1}^3 (\pi BO_{AB})_n \frac{e^{-\frac{E_n}{kT}}}{e^{-\frac{E_1}{kT}} + e^{-\frac{E_2}{kT}} + e^{-\frac{E_3}{kT}}}$$

where $(\pi BO_{AB})_n$ is the π Mayer bond order (π -MBO) of the *n*th isomer, E_n is the energy of the *n*th isomer, k is the Boltzmann constant, and T is the temperature.

Preparation of the linear oligoisindole compounds 1-4. Sodium metal (25 mg) was dissolved in 2.5 mL of dodecanethiol at 100 °C. After all sodium was dissolved, 4,5-bis(2,6-diisopropylphenoxy)phthalonitrile (300 mg, 0.625 mmol) was added and the

mixture was stirred for 1 h at the same temperature. Then, the reaction temperature was elevated to 180 °C and stirred for 1 h. After cooling to room temperature, the reaction solution was applied on a silica gel column for chromatography. CHCl₃/*n*-hexane = 1/1 (v/v) first eluted a yellowish band containing diisoindole **1**, which was followed by the second blue band containing phthalocyanine (24.3mg, 8.1%), the third orange band containing triisoindole derivative **2**, the fourth red band containing tetraisoindole compound **3**. Further elution led to the isolation of trace amount of hexaisoindole compound **4**. Repeated chromatography followed by recrystallization from CHCl₃ and CH₃OH gave **1**, **2**, **3** and **4** as yellow, orange, red, and green powder in the yield of (17.1mg, 5.7%), (6.0mg, 2.0%), (24.9mg, 8.3%), and (0.6mg, 0.2%), respectively.

Compound **1**. ¹H NMR (CD₂Cl₂, 400 MHz): 7.77 (s, 2 H), 7.27-7.23 (m, 12 H), 6.42 (s, 2 H), 3.16-3.13 (m, 8 H), 2.81 (t, 4 H, *J* = 4 Hz), 1.25-1.06 (m, 88 H), 0.86 (t, 6 H, *J* = 4 Hz); ¹³C NMR (CDCl₃, 100 MHz): δ 171.2, 149.5, 148.7, 148.5, 148.4, 144.7, 141.8, 141.7, 133.4, 131.6, 126.3, 126.1, 124.8, 124.6, 111.5, 104.6, 32.0, 31.0, 29.7, 29.7, 29.6, 29.4, 29.4, 29.3, 29.2, 28.3, 28.0, 27.3, 23.9, 22.8, 22.8, 13.9, 0.9; UV/Vis (CHCl₃): λ_{max} (logε)= 284 (4.57), 353 (3.88), 432 (4.45), 455 nm (4.49); HR MS: an isotopic cluster peaking at *m/z* 1335.8918, Calcd. for C₈₈H₁₂₃N₂O₄S₂, [*M*+*H*]⁺ 1335.8919.

Compound **2**. ¹H NMR (CD₂Cl₂, 400 MHz): 9.84 (br, 1H), 7.92 (s, 1 H), 7.41-7.23 (m, 19 H), 6.85 (s, 1 H), 6.67 (s, 1 H), 6.59 (s, 1 H), 6.44 (s, 1 H), 4.05 (s, 2H), 3.16-3.10 (m, 12 H), 2.70 (t, 2 H, *J* = 4 Hz), 1.25-1.07 (m, 92 H), 0.85 (t, 3 H, *J* = 4 Hz); ¹³C NMR (CDCl₃, 100 MHz): δ 165.0, 151.4, 149.4, 148.9, 148.7, 148.6, 148.5, 148.3, 148.1, 142.0, 141.8, 141.7, 141.6, 141.3, 136.4, 131.8, 126.2, 126.0, 125.8, 124.7, 124.5, 124.3, 108.7, 108.1, 107.3, 104.6, 31.0, 30.6, 29.7, 29.6, 29.3, 28.2, 27.8, 27.3, 27.2, 27.1, 24.0, 23.8, 23.2, 22.7, 14.1, 1.0; UV/Vis (CHCl₃): λ_{max} (logε)= 284 (4.77), 352 (4.31), 476 (4.62), 501

(4.59), 534 nm (4.34); HR MS: an isotopic cluster peaking at m/z 1618.0259, Calcd. for $C_{108}H_{137}N_4O_6S$, $[M+H]^+$ 1618.0253.

Compound **3**. 1H NMR (CD_2Cl_2 , 400 MHz): 9.69 (br, 2 H), 7.52 (s, 2 H), 7.37-7.08 (m, 24 H), 6.83 (s, 2 H), 6.70 (s, 2 H), 6.56 (s, 2 H), 3.96 (s, 4 H), 3.19-3.12 (m, 16 H), 1.12-1.06 (m, 96 H); ^{13}C NMR ($CDCl_3$, 100 MHz): δ 149.1, 148.9, 148.8, 148.6, 148.5, 143.4, 142.1, 141.8, 141.7, 141.5, 136.4, 133.1, 132.4, 128.4, 126.4, 126.3, 125.9, 125.4, 124.8, 124.7, 124.6, 124.4, 109.7, 108.3, 107.4, 106.7, 27.5, 27.4, 27.3, 24.3, 23.8, 23.3, 22.9; UV/Vis ($CHCl_3$): λ_{max} (log ϵ) = 345 (4.42), 492 (4.59), 522 (4.72), 559 nm (4.64); HR MS: an isotopic cluster peaking at m/z 1900.1584, Calcd. for $C_{128}H_{151}N_6O_8$, $[M-H]^+$ 1900.1588.

Compound **4**. 1H NMR (CD_2Cl_2 , 400 MHz): 10.02 (br, 2 H), 8.85 (br, 1 H), 7.52 (s, 2 H), 7.42-7.19 (m, 30 H), 6.92 (m, 4 H), 6.74 (s, 2 H), 6.62-6.57 (m, 6 H), 6.31 (m, 4 H), 4.17 (s, 4 H), 3.47-2.98 (m, 24 H), 1.33-0.72 (m, 144 H); HR MS: an isotopic cluster peaking at m/z 2846.7122, Calcd. for $C_{192}H_{223}N_9O_{12}$, $[M]^+$ 2846.7111.

Preparation of the linear tetraisoindole 5. By employing the above-described procedure with 4,5-bis(2,6-dimethylphenoxy)phthalonitrile instead of 4,5-bis(2,6-diisopropylphenoxy)phthalonitrile as the starting material, the linear tetraisoindole analogue **5** was isolated in the yield of 2.4%. 1H NMR (CD_2Cl_2 , 400 MHz): 9.92 (br, 2 H), 7.61 (s, 2 H), 7.26-7.08 (m, 24 H), 6.61 (s, 2 H), 6.57 (s, 2 H), 6.50 (s, 2 H), 4.21 (s, 4 H), 2.24-2.16 (m, 48H); ^{13}C NMR ($CDCl_3$, 100 MHz): δ 170.1, 164.4, 151.9, 151.1, 150.9, 150.7, 150.1, 147.8, 147.5, 147.3, 143.2, 136.7, 133.0, 132.8, 131.2, 131.0, 129.3, 129.2, 129.0, 128.3, 125.6, 125.5, 125.2, 124.7, 110.3, 107.9, 107.0, 106.3, 50.1, 16.3, 16.2, 16.2; UV/Vis ($CHCl_3$): λ_{max} (log ϵ)= 344 (4.50), 491 (4.67), 520 (4.80), 556 nm

(4.71); HR MS: an isotopic cluster peaking at m/z 1451.6571, Calcd. for $C_{96}H_{87}N_6O_8$, $[M-H]^+$ 1451.6580.

References

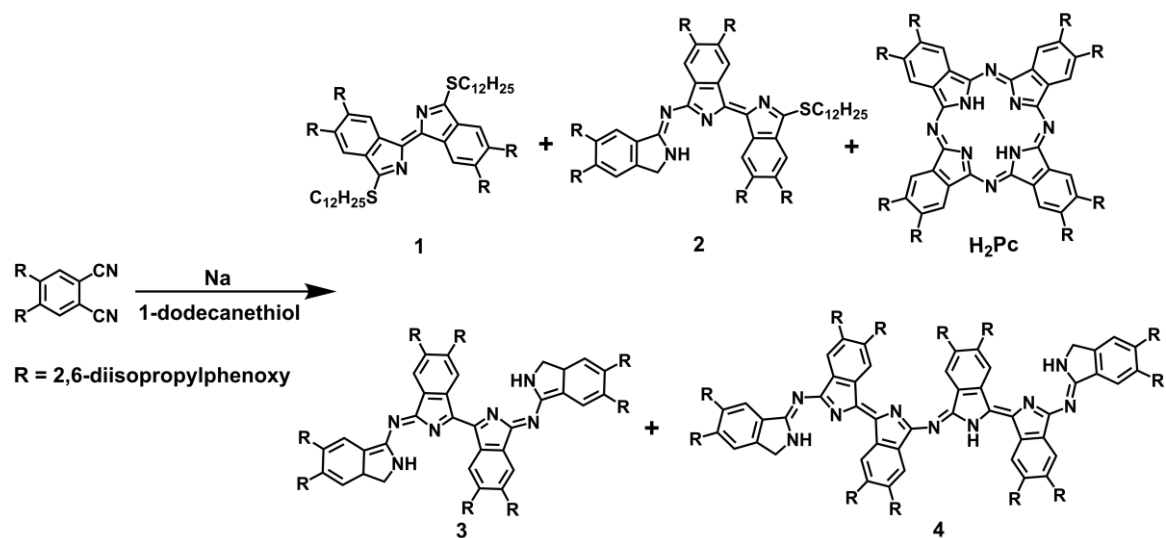
- 1 H. Shang, H. Wang, W. Li and J. Jiang, *Vib. Spectrosc.*, 2013, **69**, 8.
- 2 S. Dong, D. Qi, Y. Zhang, J. Jiang and Y. Bian, *Vib. Spectrosc.*, 2011, **56**, 245.
- 3 J. Jiang, M. Bao, L. Rintoul and D. P. Arnold, *Coord. Chem. Rev.*, 2006, **250**, 424 and references therein.
- 4 (a) H. Pan, C. Chen, K. Wang, W. Li and J. Jiang, *Chem. Eur. J.*, 2015, **21**, 3168; (b) Y. Zhang, L. Zhao, K. Wang and J. Jiang, *Inorg. Chem. Front.*, 2017, **4**, 104.
- 5 H. Pan, W. Liu, C. Wang, K. Wang and J. Jiang, *Chem. Eur. J.*, 2016, **22**, 9488.
- 6 R. H. Blessing, *Acta Crystallogr.*, 1995, **A51**, 33.
- 7 *SHELXL Reference Manual*, Version 5.1; Bruker Analytical X-Ray Systems: Madison, WI, 1997.
- 8 Gaussian 09, Revision D.01, M. J. Frisch, G. W. Trucks, H. B. Schlegel, G. E. Scuseria, M. A. Robb, J. R. Cheeseman, G. Scalmani, V. Barone, B. Mennucci, G. A. Petersson, H. Nakatsuji, M. Caricato, X. Li, H. P. Hratchian, A. F. Izmaylov, J. Bloino, G. Zheng, J. L. Sonnenberg, M. Hada, M. Ehara, K. Toyota, R. Fukuda, J. Hasegawa, M. Ishida, T. Nakajima, Y. Honda, O. Kitao, H. Nakai, T. Vreven, J. A. Montgomery, Jr., J. E. Peralta, F. Ogliaro, M. Bearpark, J. J. Heyd, E. Brothers, K. N. Kudin, V. N. Staroverov, T. Keith, R. Kobayashi, J. Normand, K. Raghavachari, A. Rendell, J. C. Burant, S. S. Iyengar, J. Tomasi, M. Cossi, N. Rega, J. M. Millam, M. Klene, J. E. Knox, J. B. Cross, V. Bakken, C. Adamo, J. Jaramillo, R. Gomperts, R. E. Stratmann, O. Yazyev, A. J. Austin, R. Cammi, C. Pomelli, J. W. Ochterski, R. L. Martin, K. Morokuma, V. G.

Zakrzewski, G. A. Voth, P. Salvador, J. J. Dannenberg, S. Dapprich, A. D. Daniels, O. Farkas, J. B. Foresman, J. V. Ortiz, J. Cioslowski, and D. J. Fox, Gaussian, Inc., Wallingford CT, 2013.

9 I. Mayer, *Chem. Phys. Lett.*, **1983**, 97, 270.

10 D. Qi and J. Jiang, *Int. J. Quantum Chem.*, **2013**, 113, 2605.

11 R. Ditchfield, W. J. Hehre and J. A. Pople, *J. Chem. Phys.*, **1971**, 54, 724.



Scheme S1 Synthesis of linear oligoisoindole compounds **1-4** along with the cyclic tetraisoindole Pc.

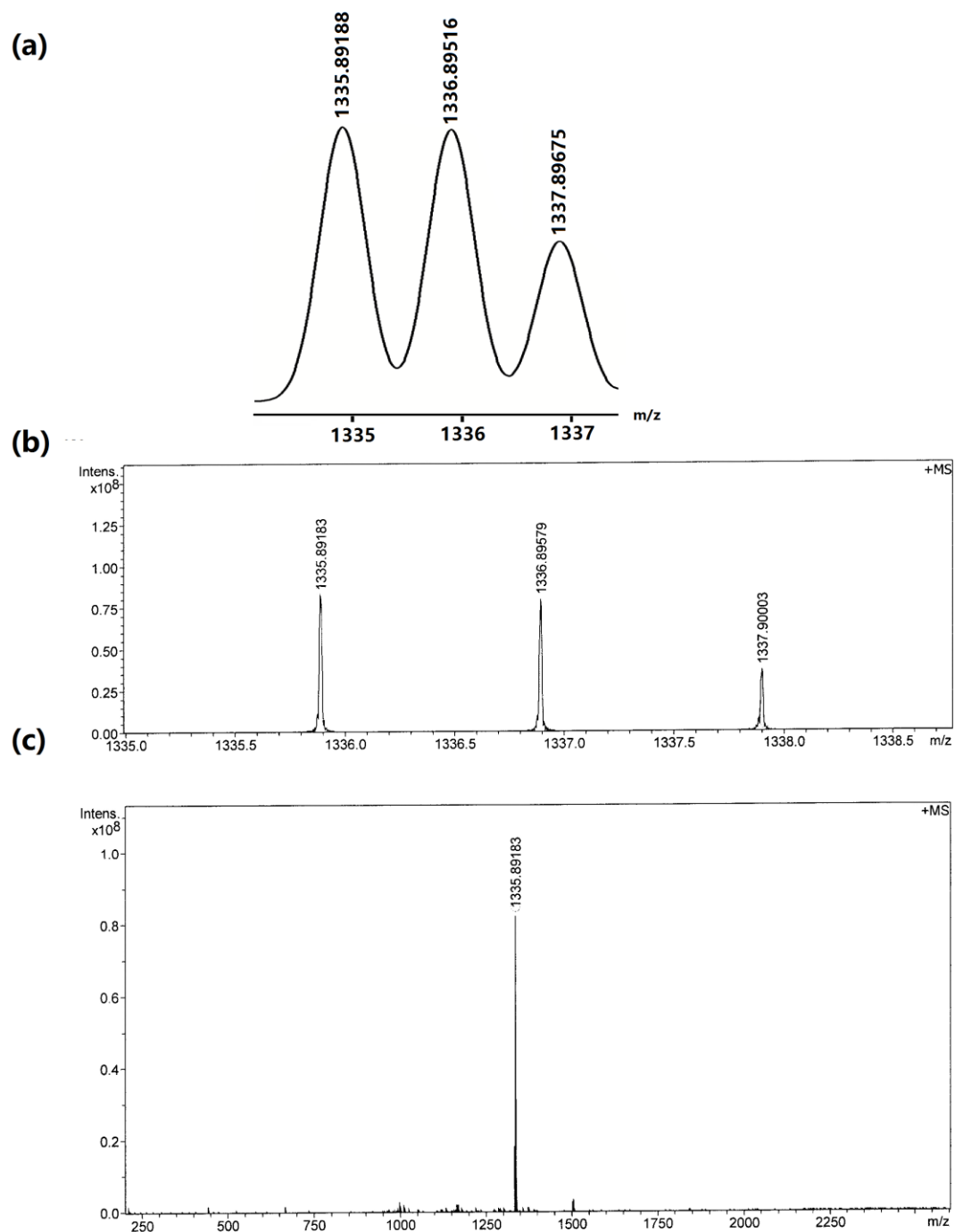


Fig. S1 Simulated (a) and experimental isotopic (b) pattern of $[M+H]^+$ and HR MS (c) for **1**.

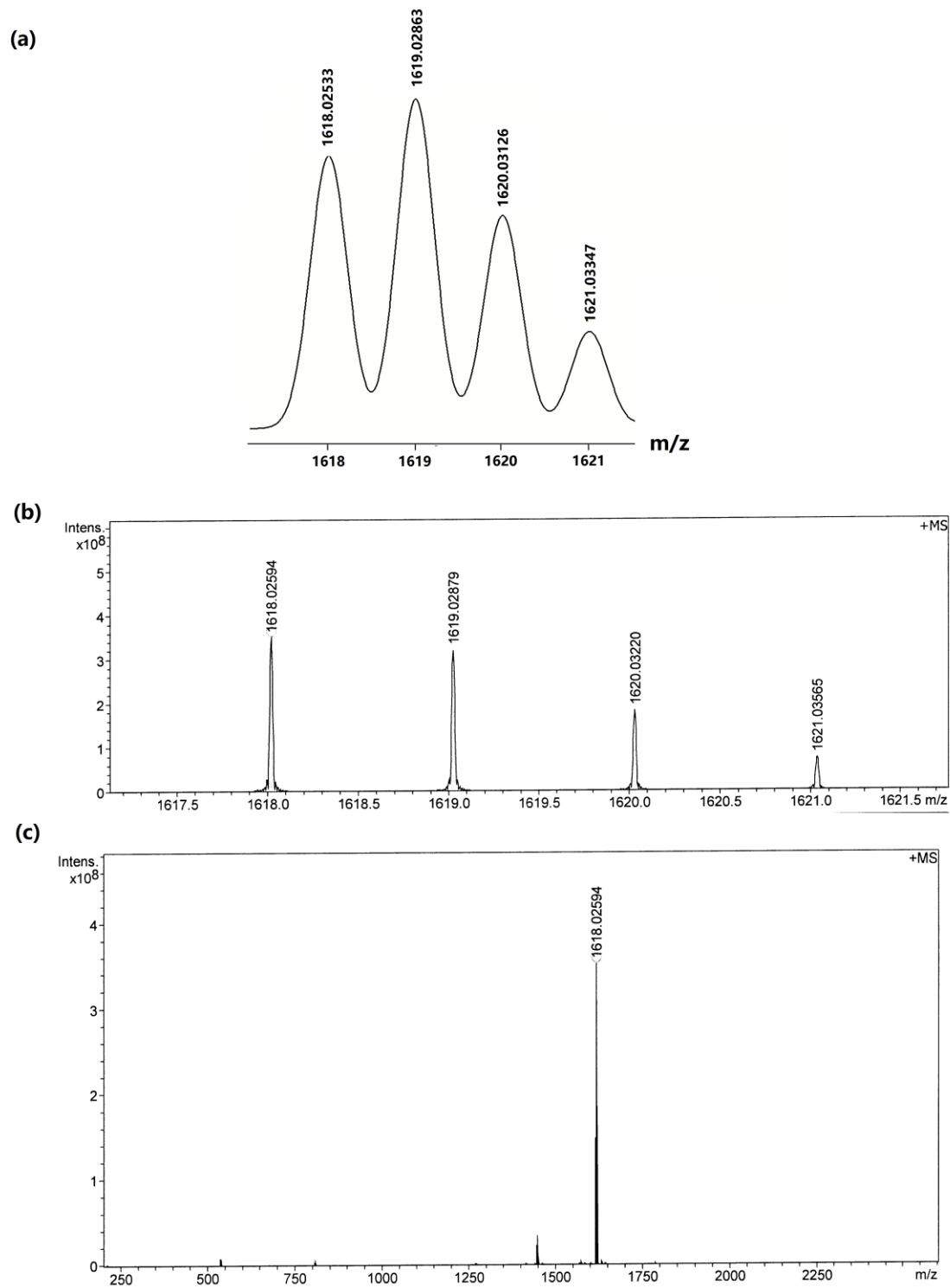


Fig. S2 Simulated (a) and experimental isotopic (b) pattern of $[M+H]^+$ and HR MS (c) for **2**.

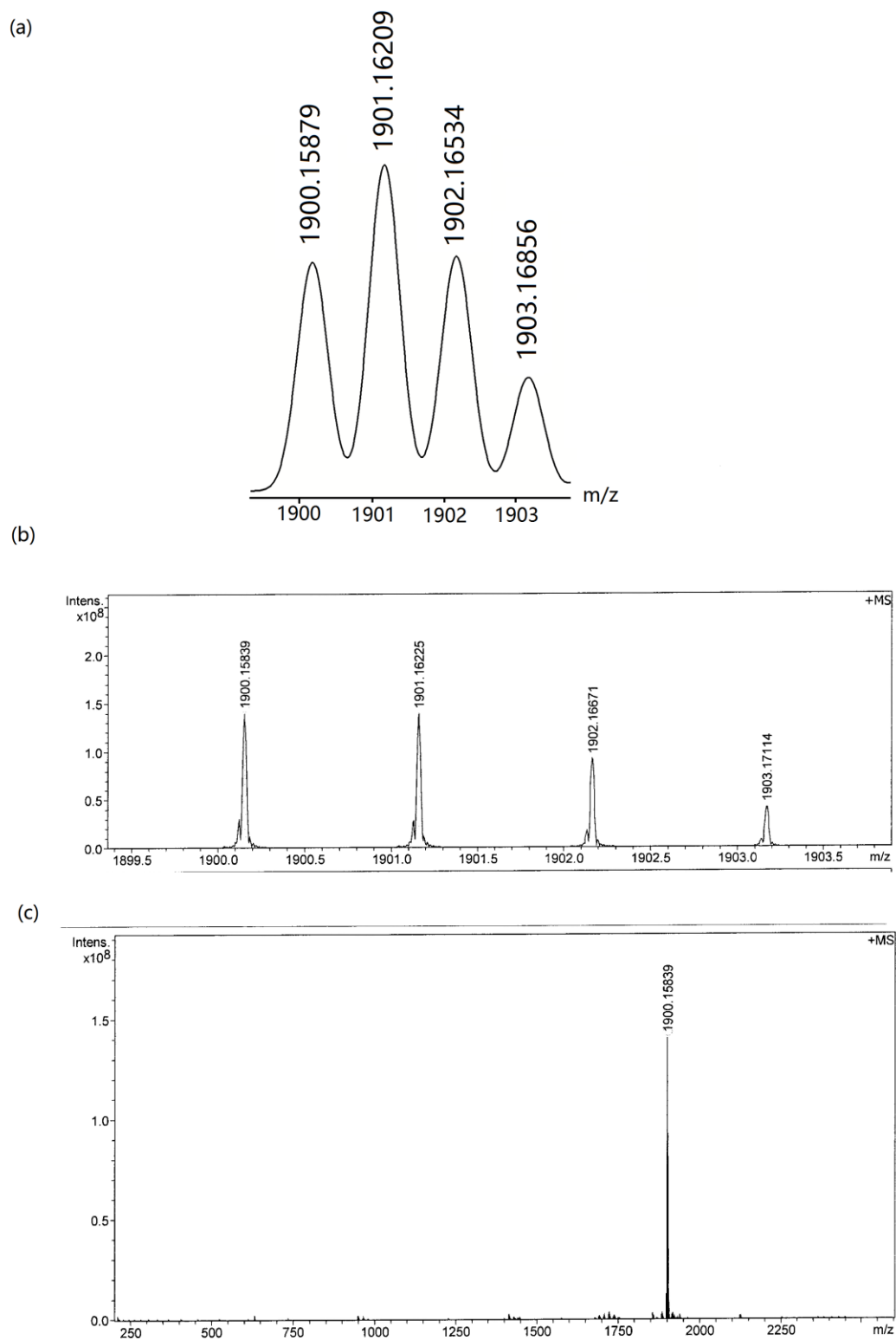


Fig. S3 Simulated (a) and experimental isotopic (b) pattern of $[M-H]^+$ and HR MS (c) for **3**.

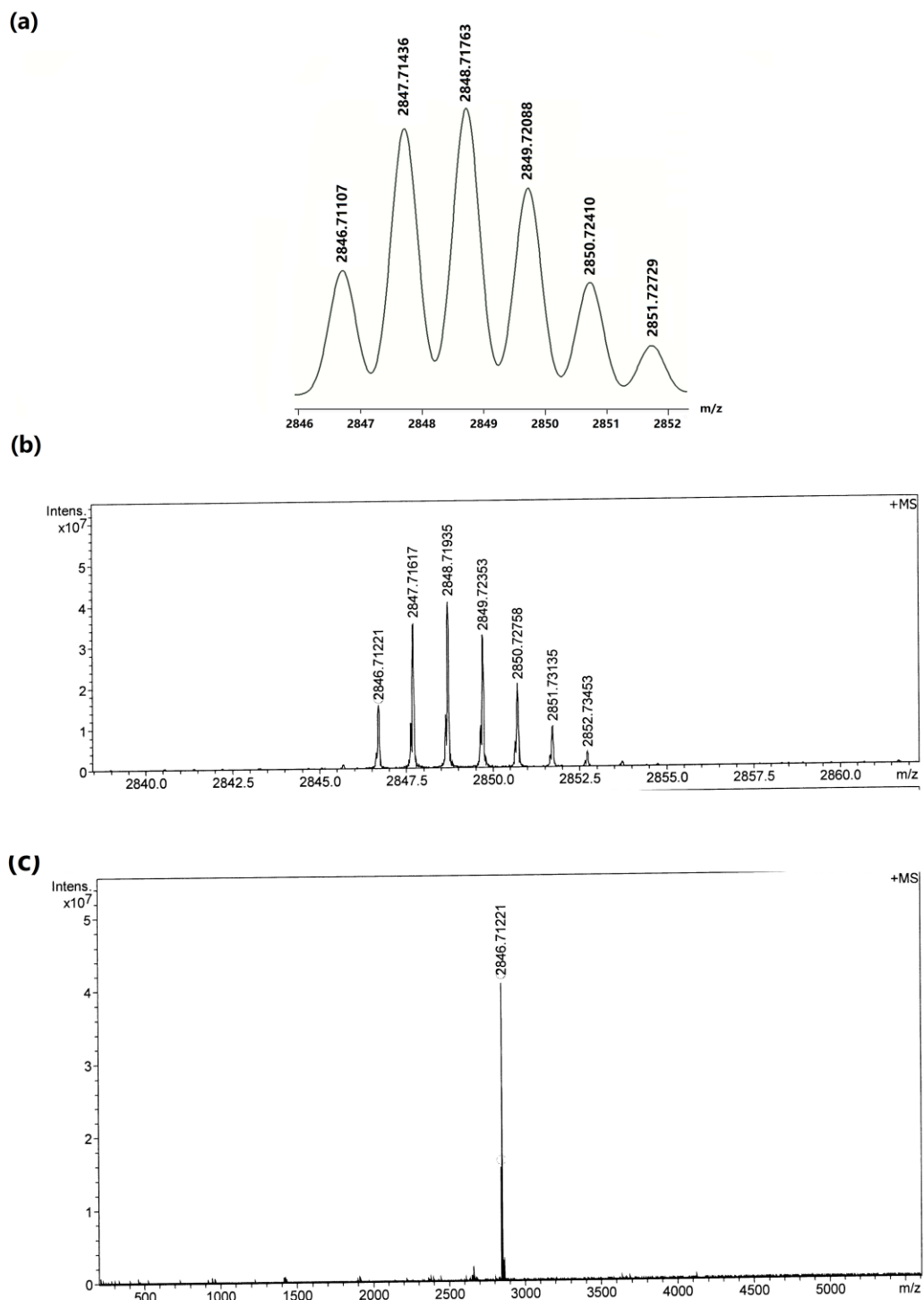


Fig. S4 Simulated (a) and experimental isotopic (b) pattern of $[M]^+$ and HR MS (c) for **4**.

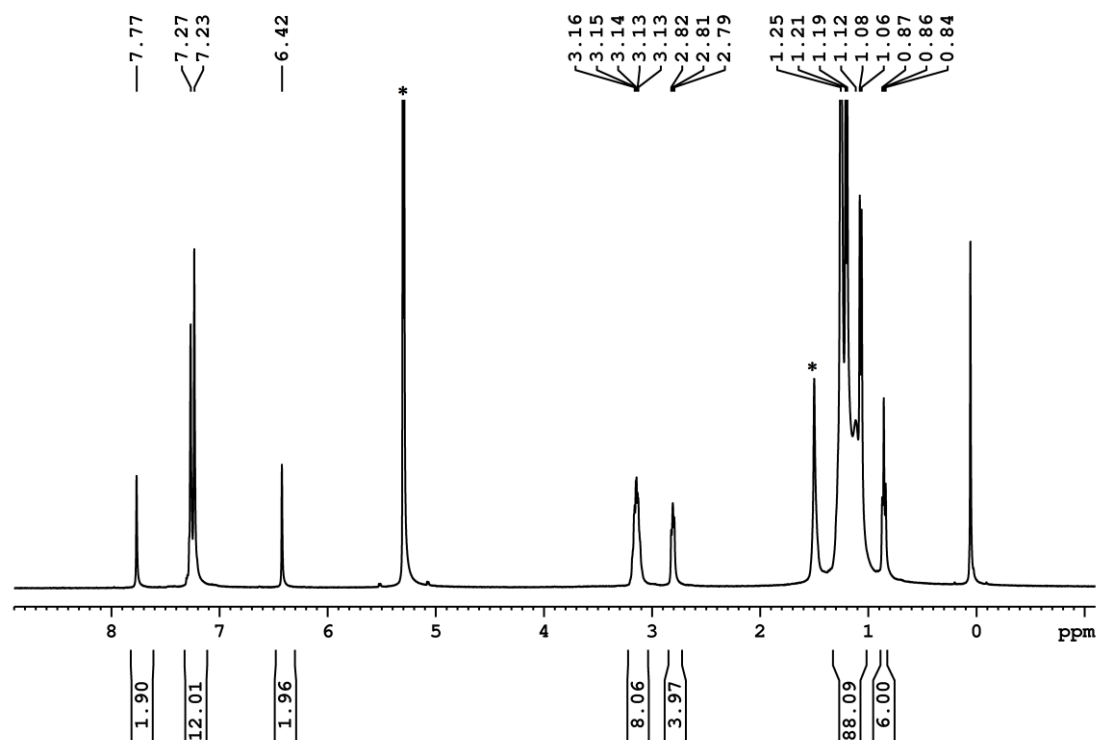


Fig. S5 ^1H NMR spectrum of **1** in CD_2Cl_2 at 298K; * indicates the signals for residual solvents.

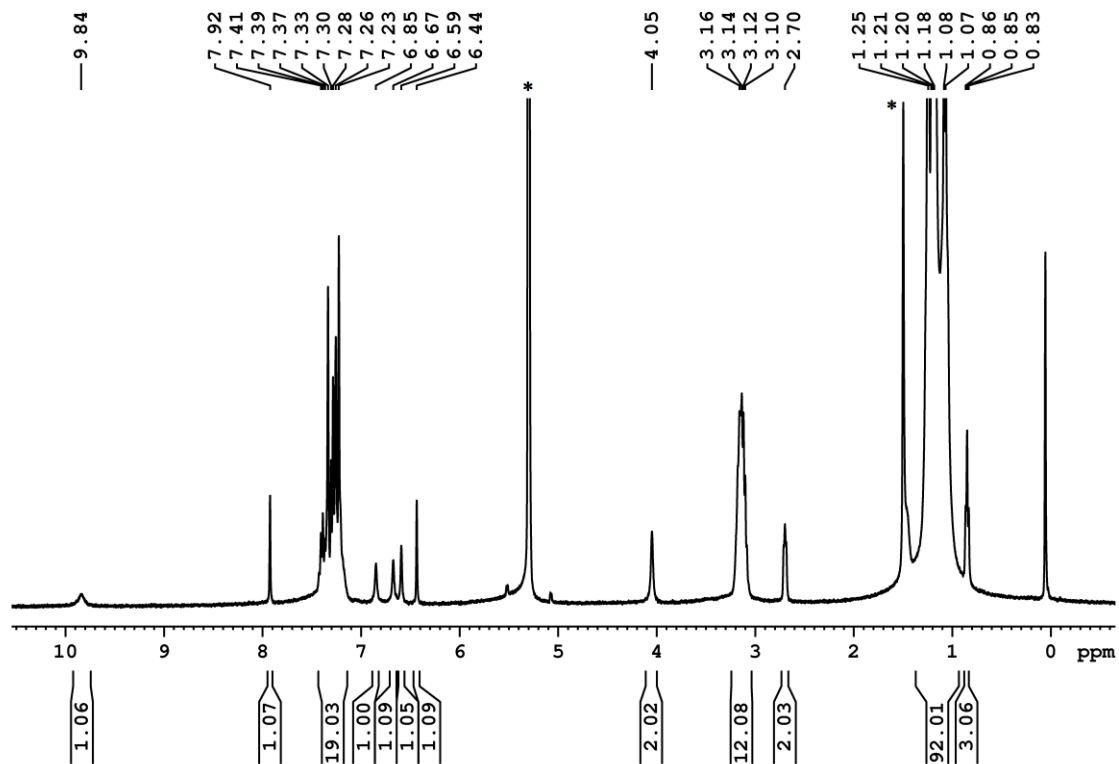


Fig. S6 ^1H NMR spectrum of **2** in CD_2Cl_2 at 298K; * indicates the signals for residual solvents.

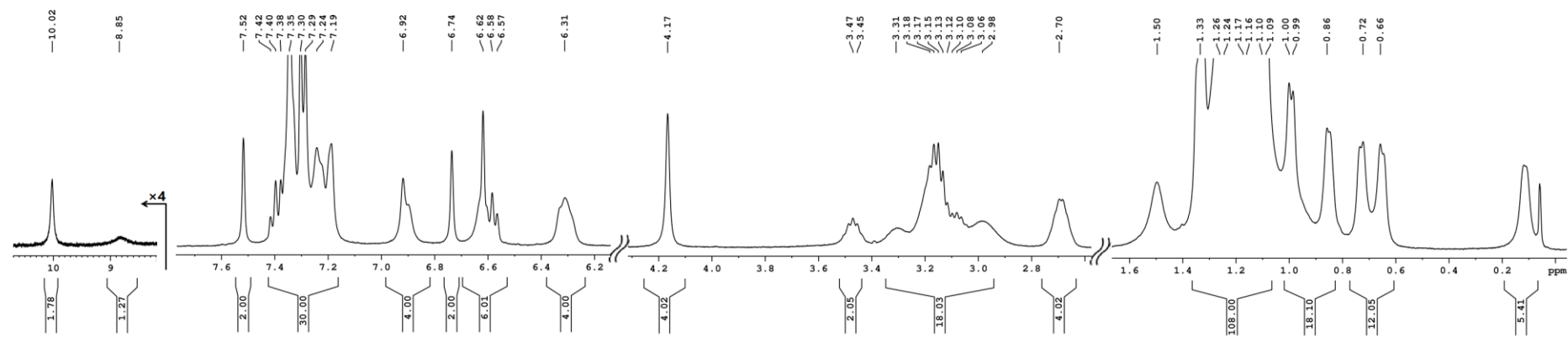


Fig. S7 ^1H NMR spectrum of **4** in CD_2Cl_2 at 298K; * indicates the signals for residual solvents.

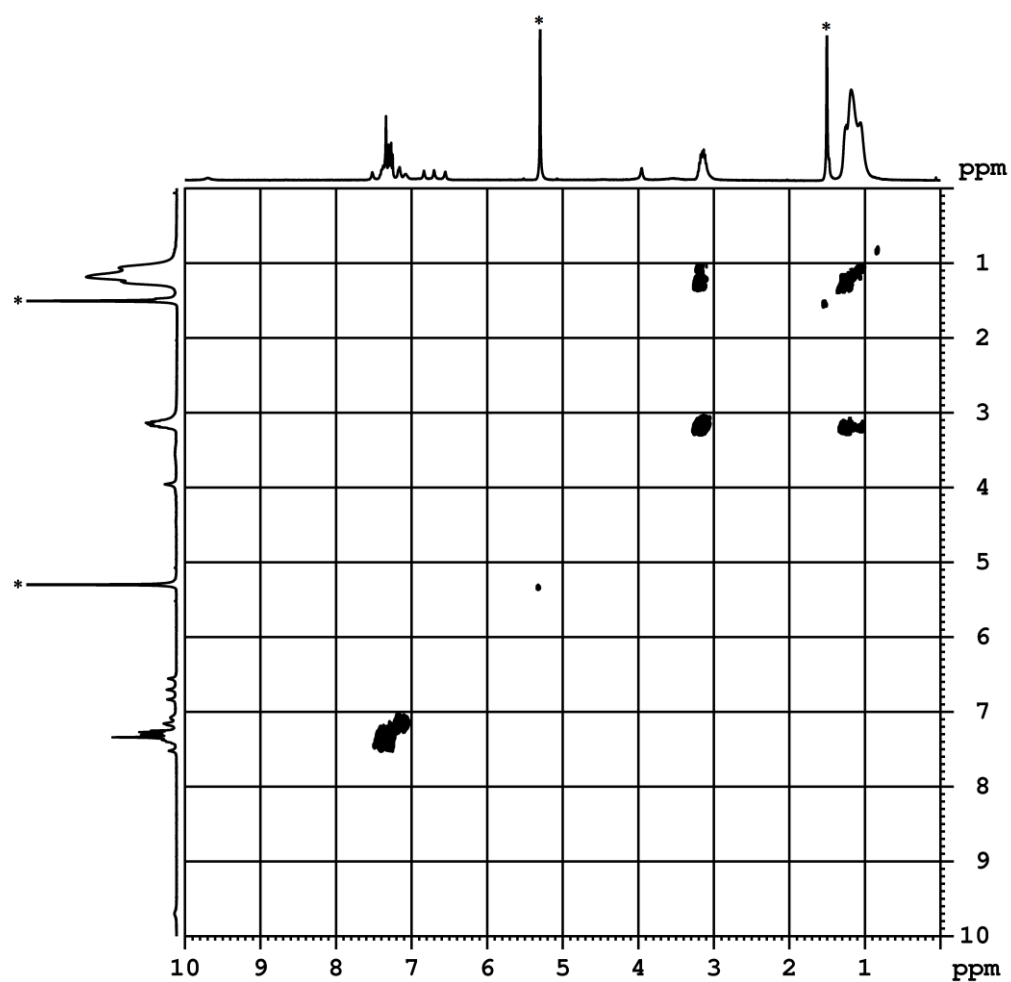


Fig. S8 ^1H - ^1H COSY spectrum of compound **3** in CD_2Cl_2 at 298K. * indicates the signals of residual solvent.

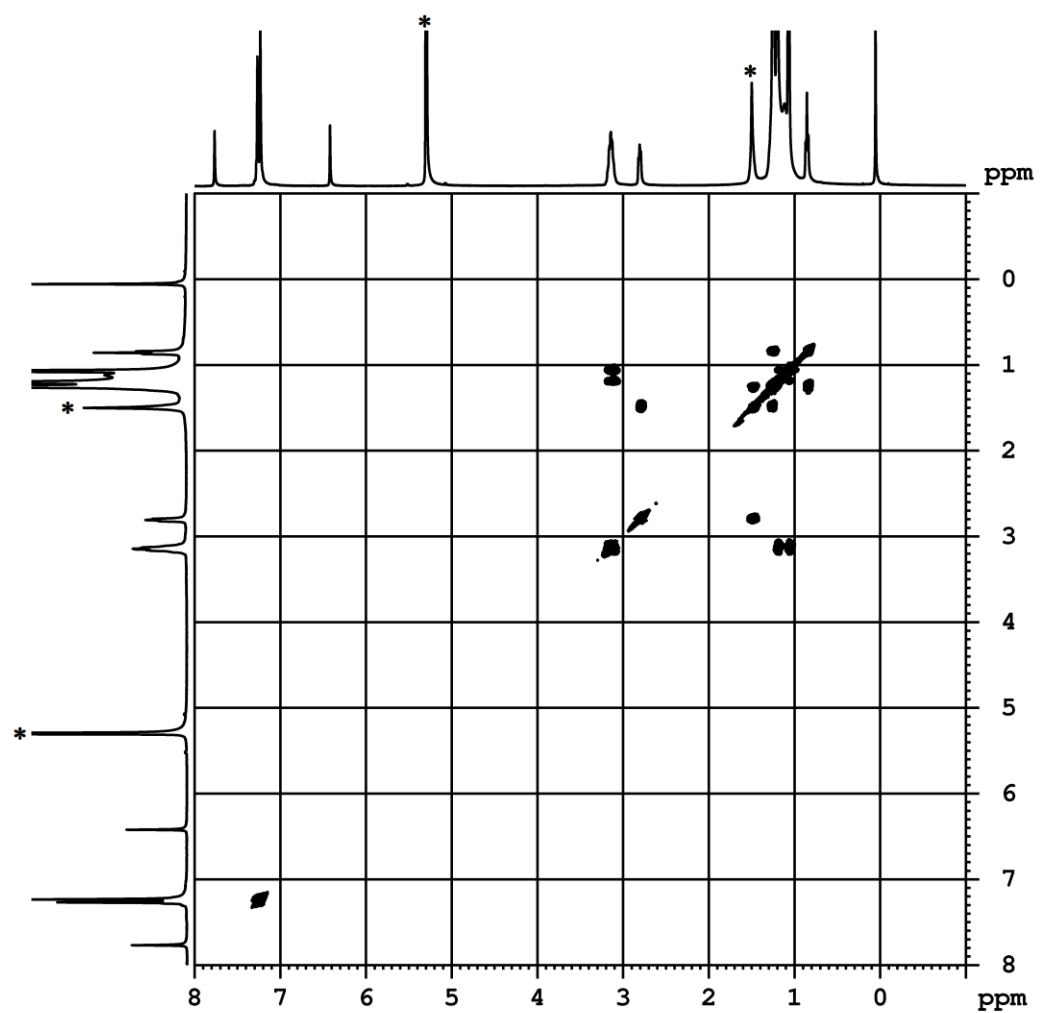


Fig. S9 ^1H - ^1H COSY spectrum of compound **1** in CD_2Cl_2 at 298K. * indicates the signals of residual solvent.

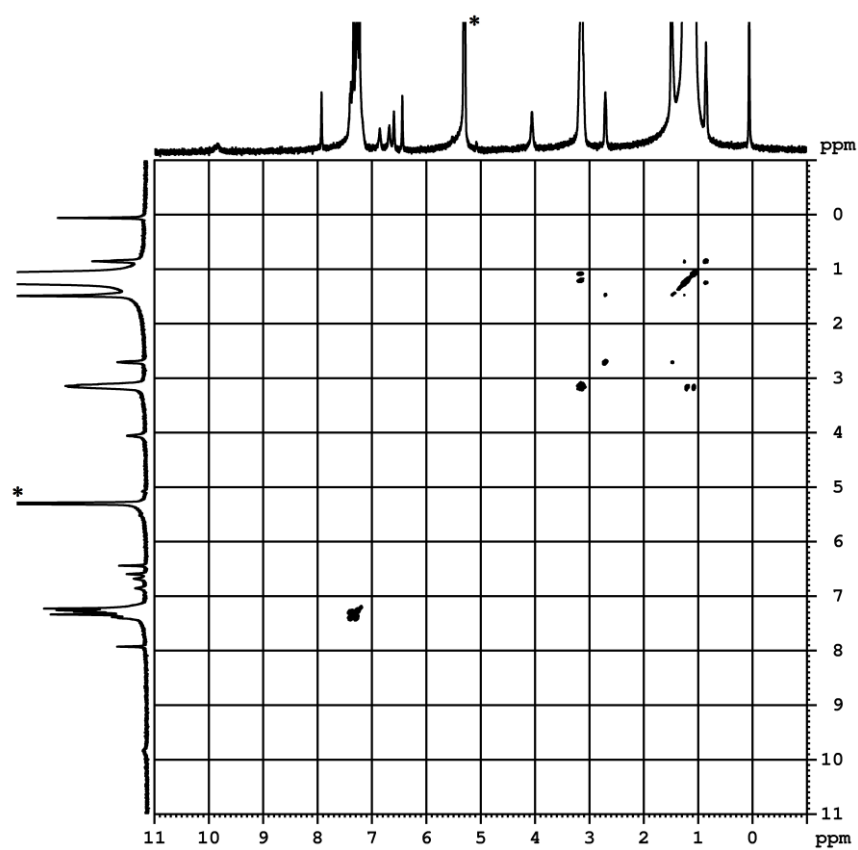


Fig. S10 ^1H - ^1H COSY spectrum of compound **2** in CD_2Cl_2 at 298K. * indicates the signals of residual solvent.

No coupling signals between the protons from the terminal carbon atoms and the N-H proton from the outer isoindole unit.

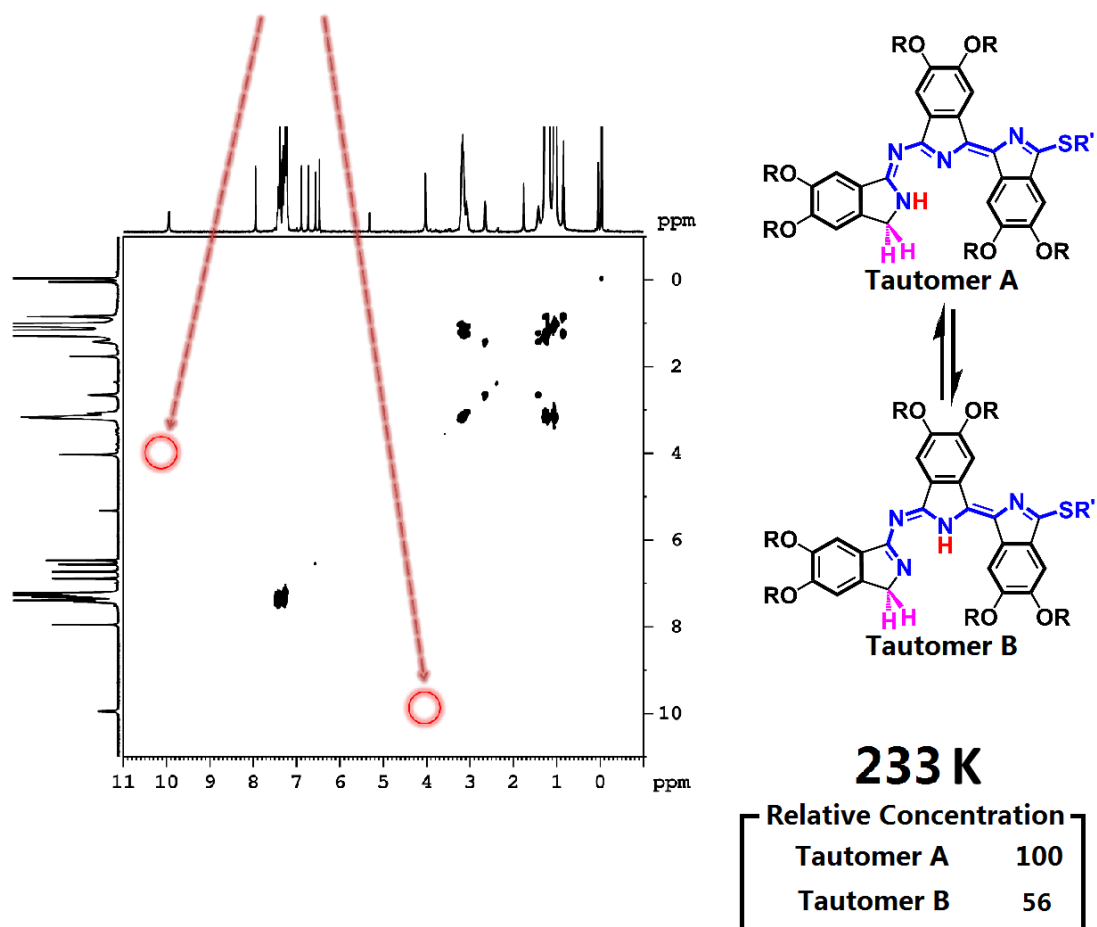


Fig. S11 ^1H - ^1H COSY spectrum of compound **2** in CDCl_3 at 233 K.

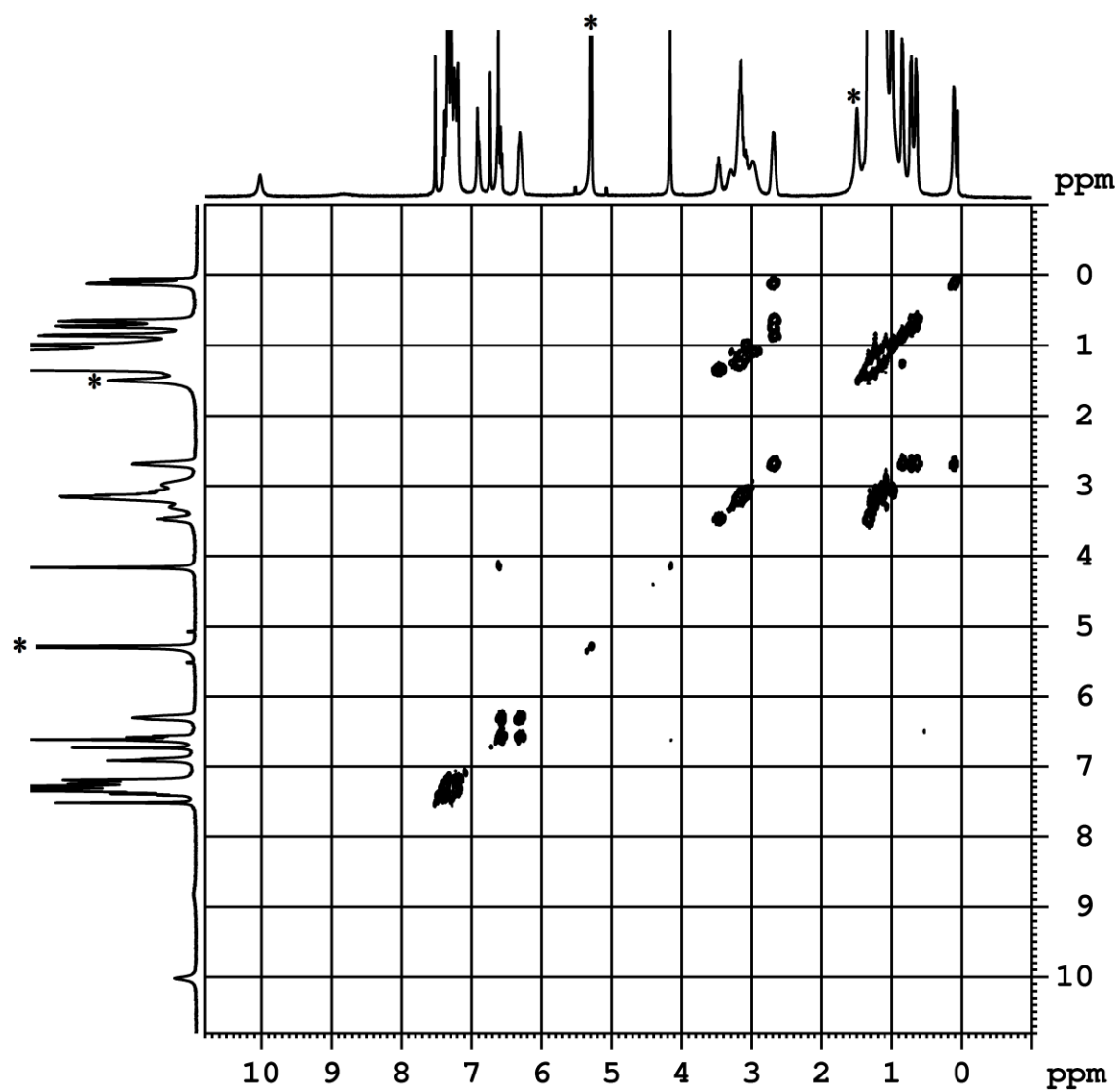


Fig. S12 ^1H - ^1H COSY spectrum of compound **4** in CD_2Cl_2 at 298 K.

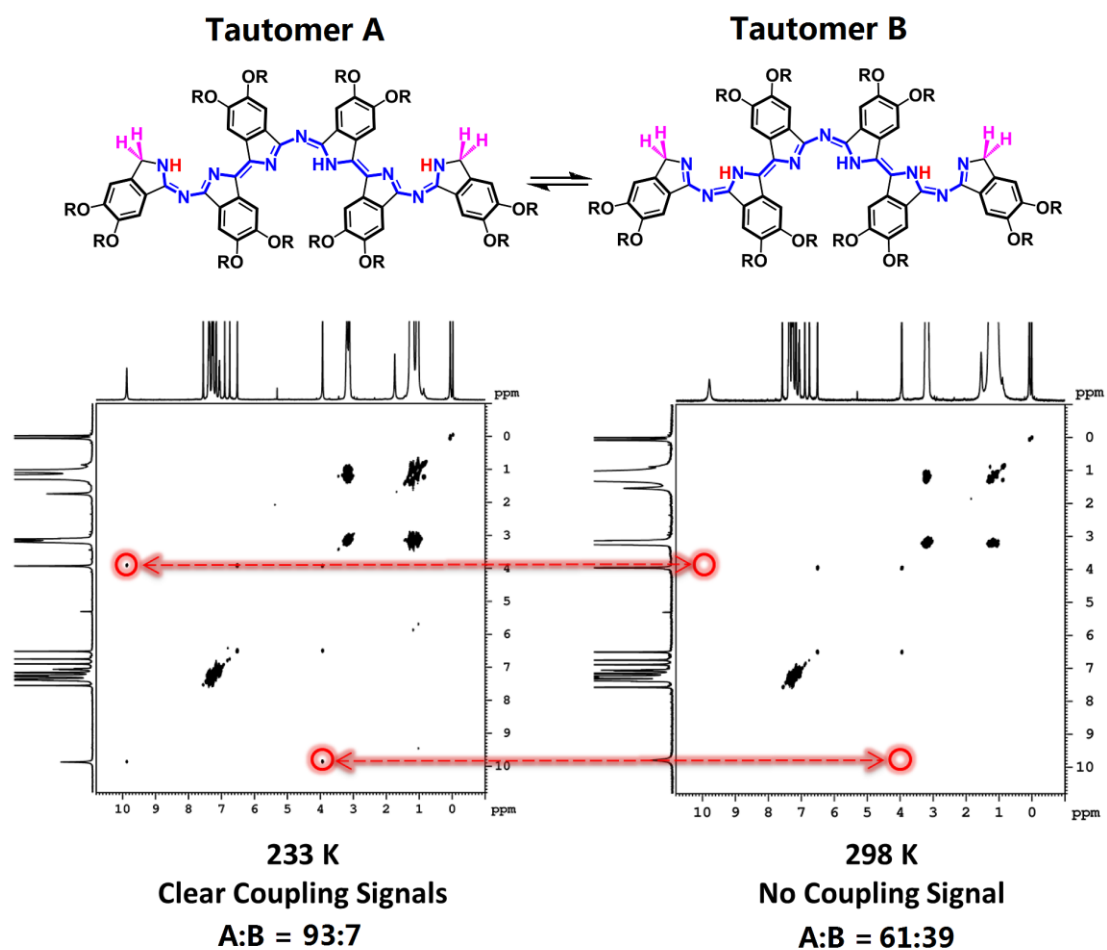


Fig. S13 Comparison of the ^1H - ^1H COSY spectra of **4** in CD_2Cl_2 recorded at 233 and 298 K.

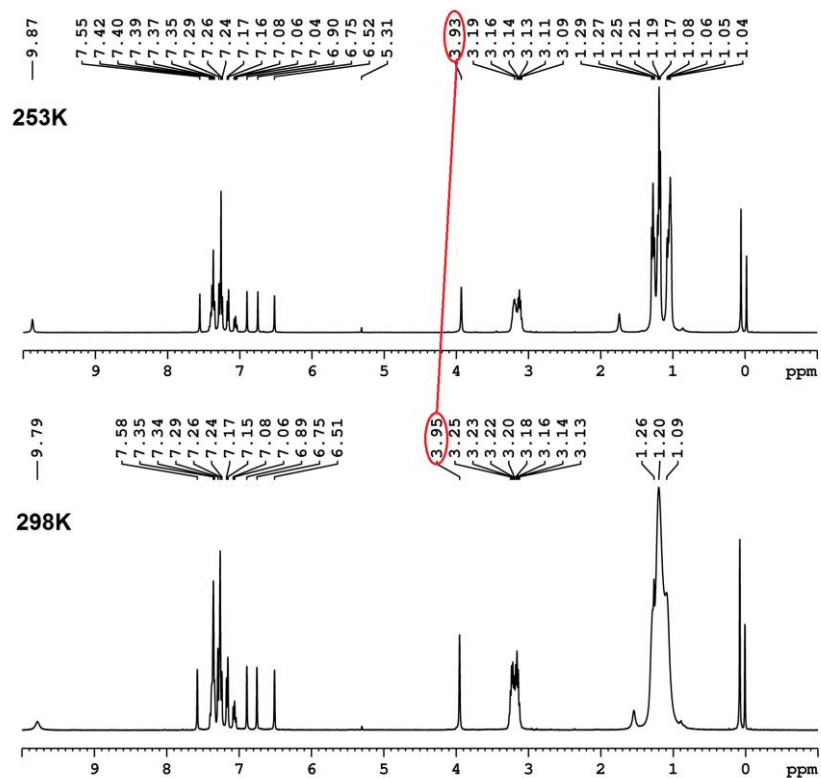


Fig. S14 Comparison of the ^1H NMR spectra of **3** in CDCl_3 recorded at 253 and 298 K.

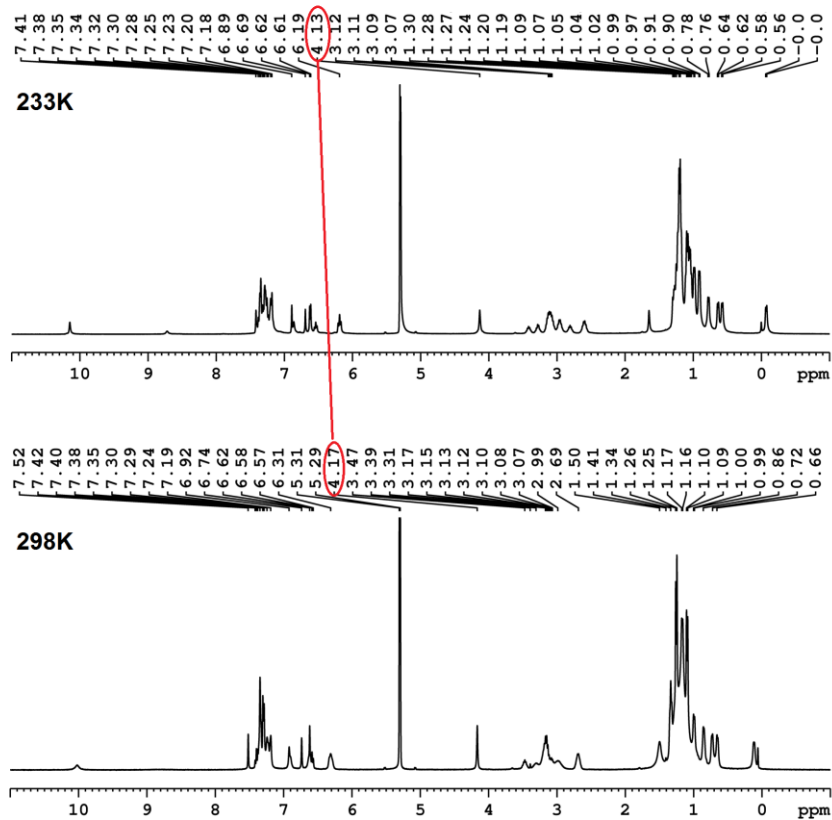


Fig. S15 Comparison of the ^1H NMR spectra of **4** in CDCl_3 recorded at 233 and 298 K.

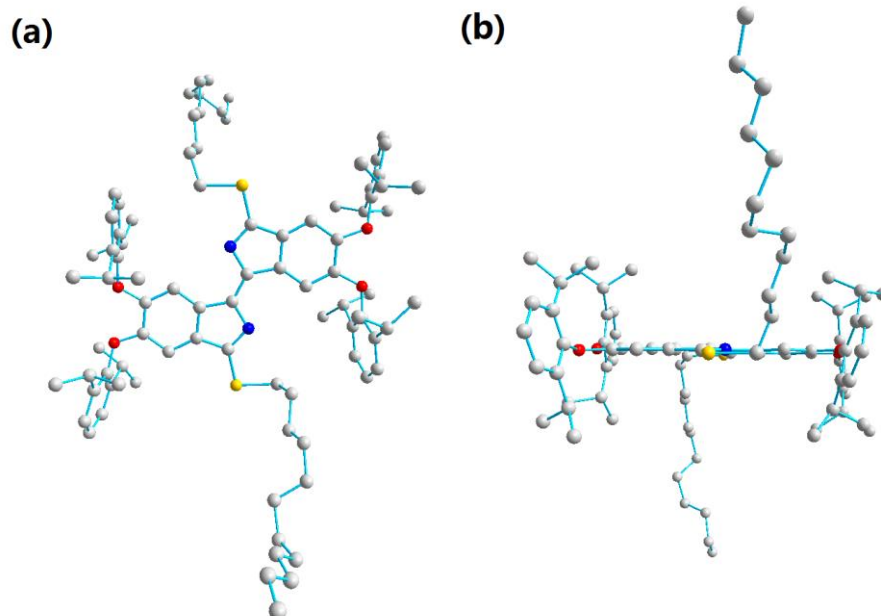


Fig. S16 Molecular structure of **1** in top view (a) and side view (b). Hydrogen atoms are omitted for clarity (C grey, N blue, O red, and S yellow).

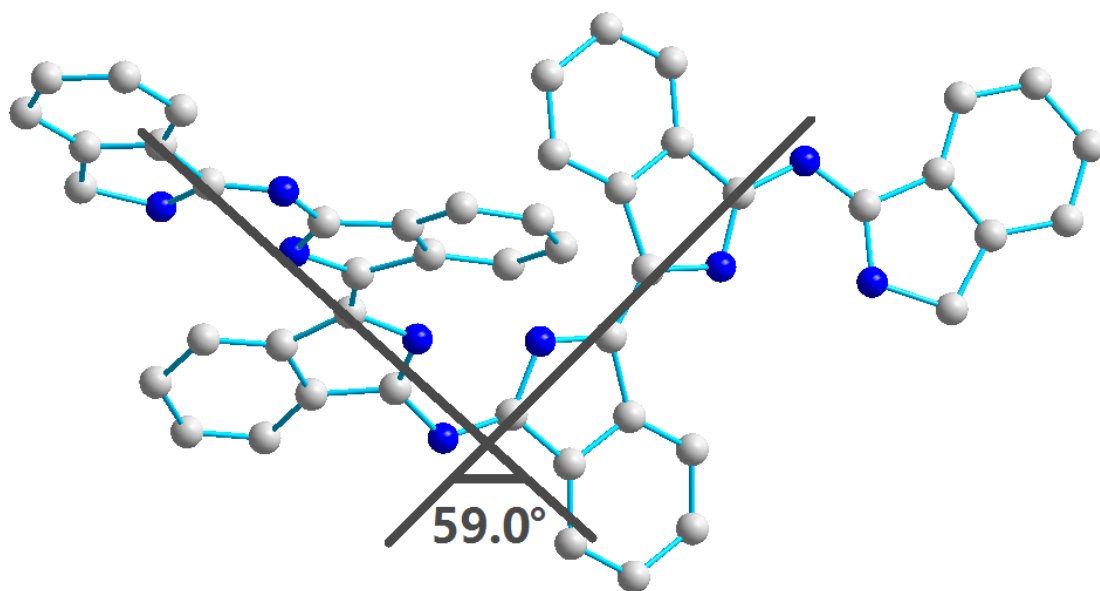


Fig. S17 The dihedral angle of the two mean planes in **4**. Substituents and hydrogen atoms are omitted for clarity (C grey and N blue).

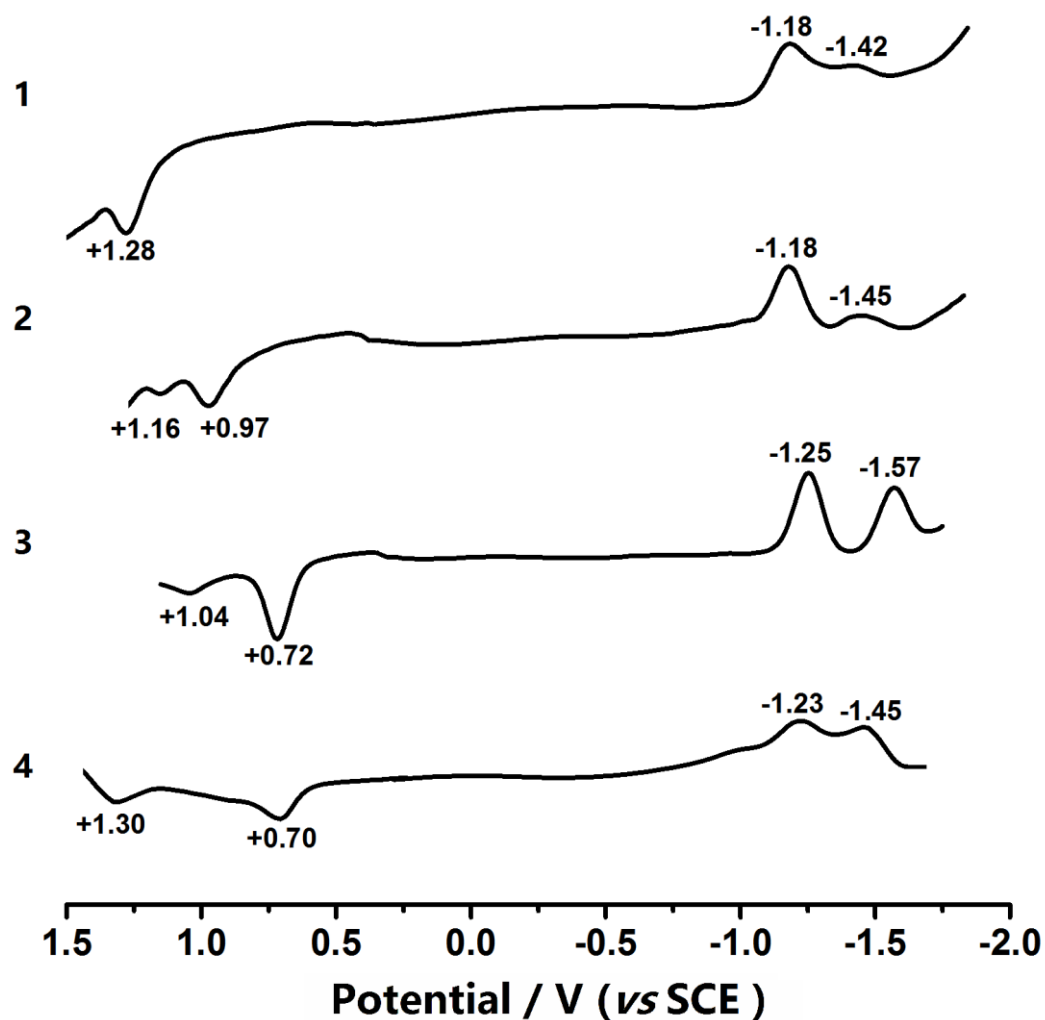


Fig. S18 Differential pulse voltammograms (DPV) for **1-4** in CH_2Cl_2 containing $0.1 \text{ mol dm}^{-3} [\text{Bu}_4\text{N}]^+[\text{ClO}_4]^-$ at a scan rate of 20 mV s^{-1} with Ag^+/Ag (a solution of 0.01 M AgNO_3 and 0.1 M TBAP in acetonitrile) as the reference electrode. It was corrected for junction potentials by being referenced internally to the ferrocenium/ferrocene (Fc^+/Fc) couple [$E_{1/2}(\text{Fc}^+/\text{Fc}) = 0.501 \text{ V vs. SCE}$].

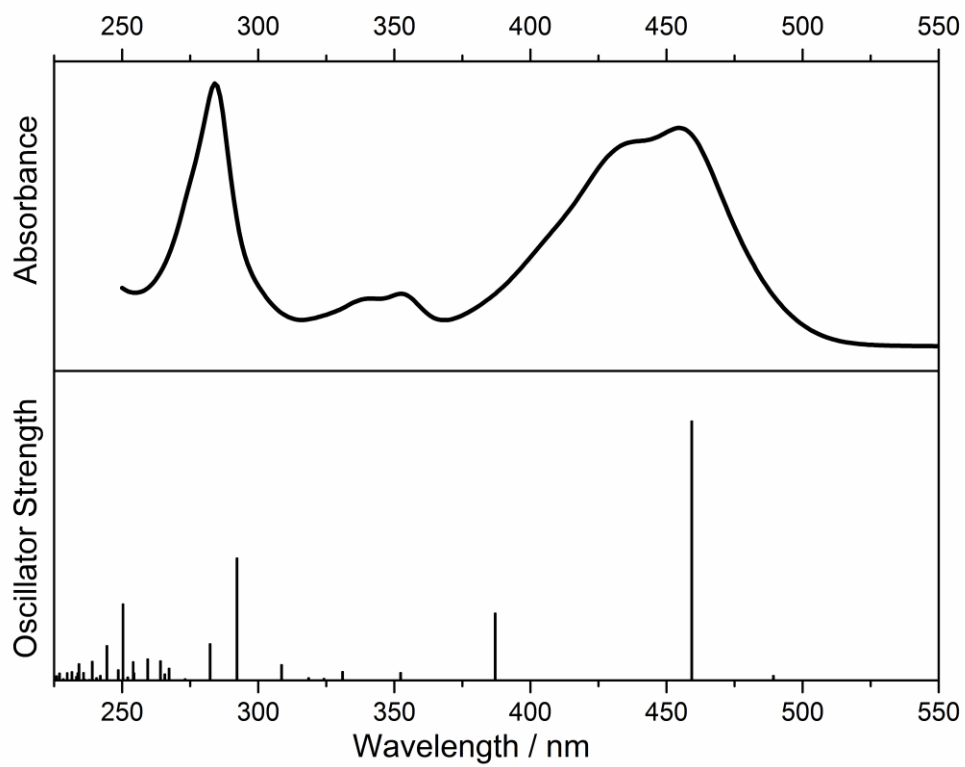


Fig. S19 The experimental and simulated electronic absorption spectra for **1**.

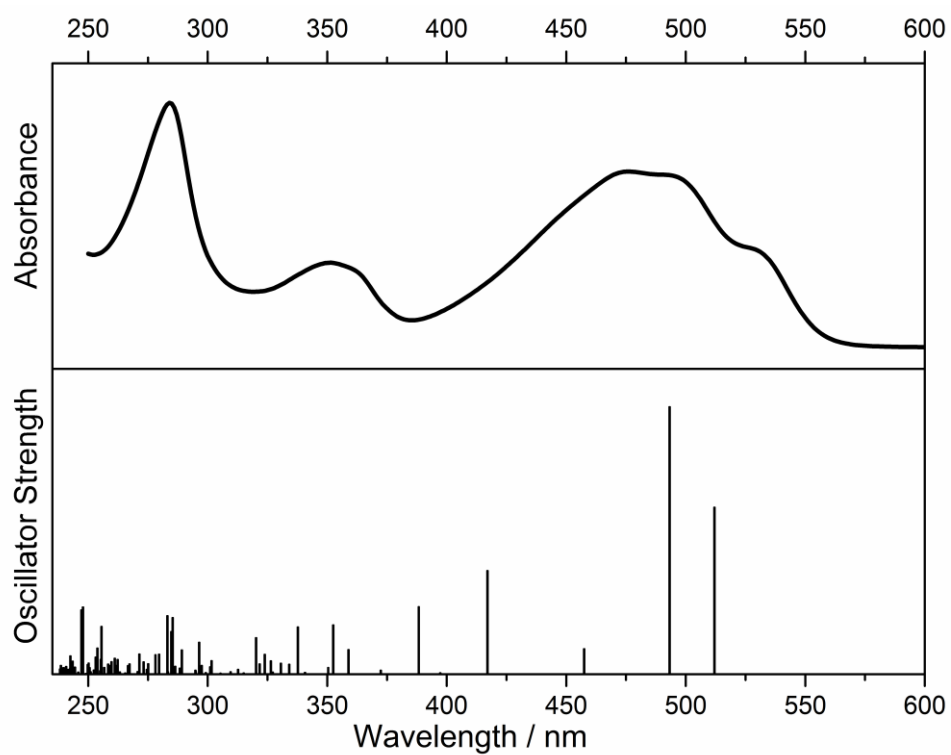


Fig. S20 The experimental and simulated electronic absorption spectra for **2**.

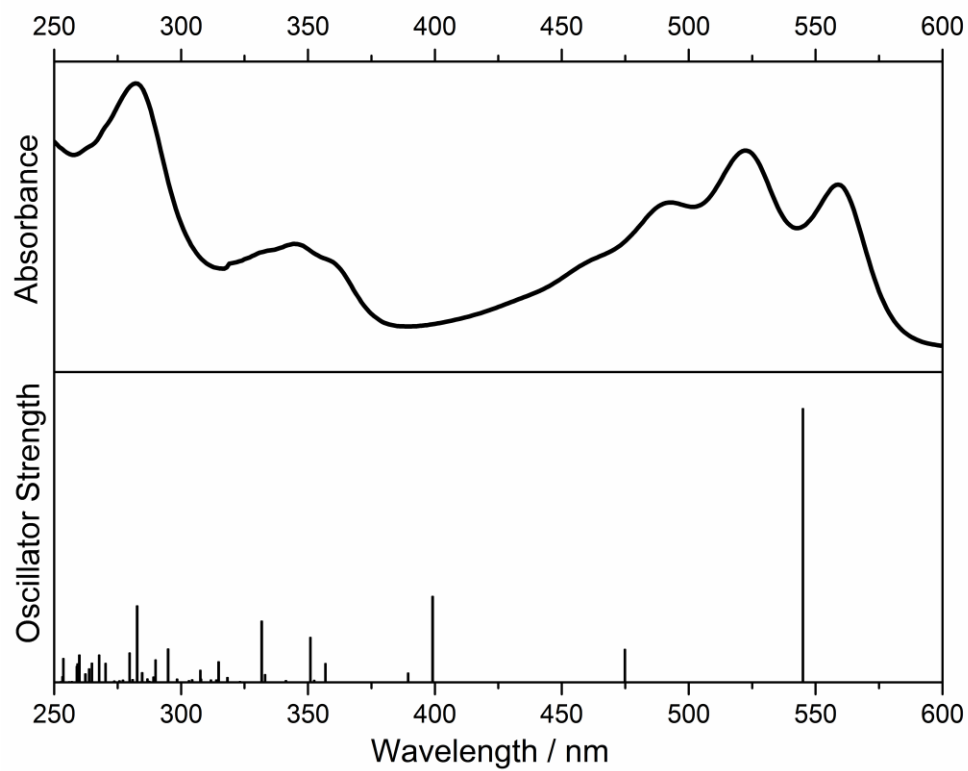


Fig. S21 The experimental and simulated electronic absorption spectra for **3**.

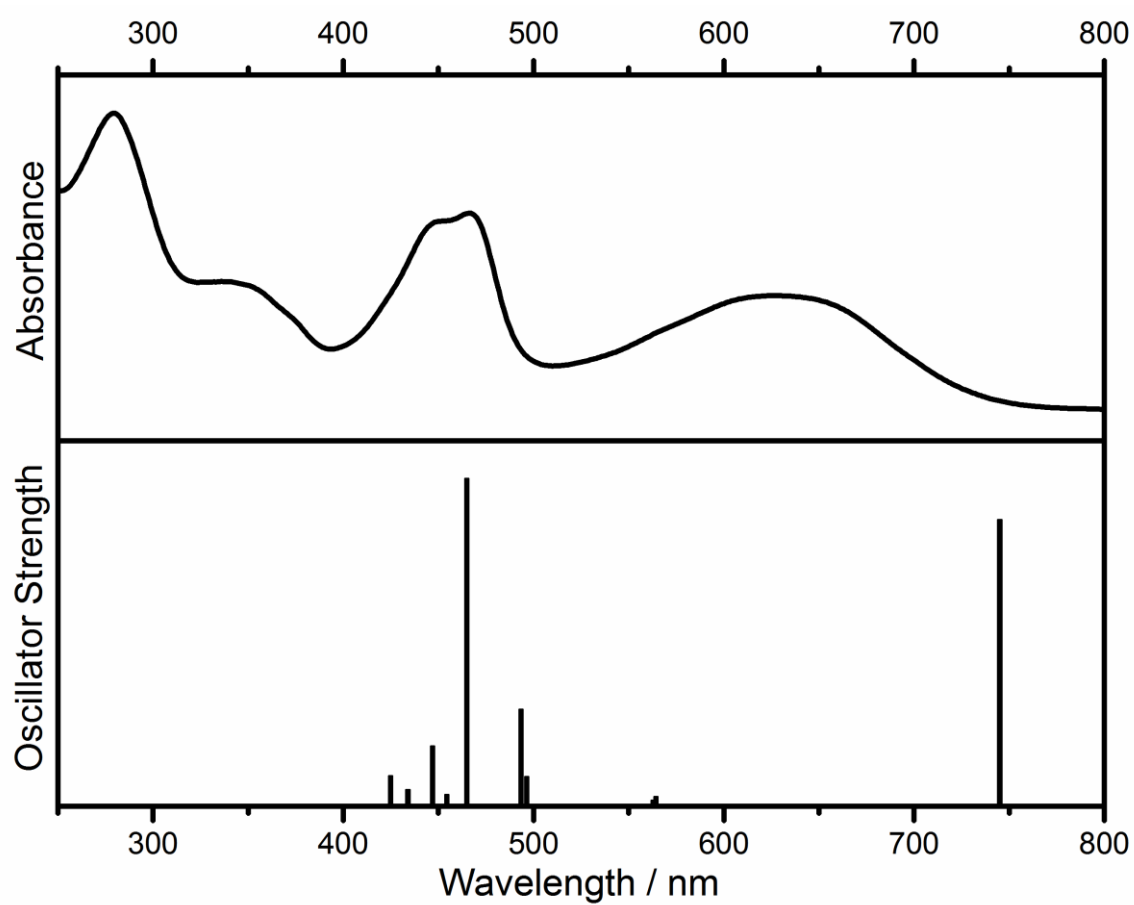


Fig. S22 The experimental and simulated electronic absorption spectra for **4**.

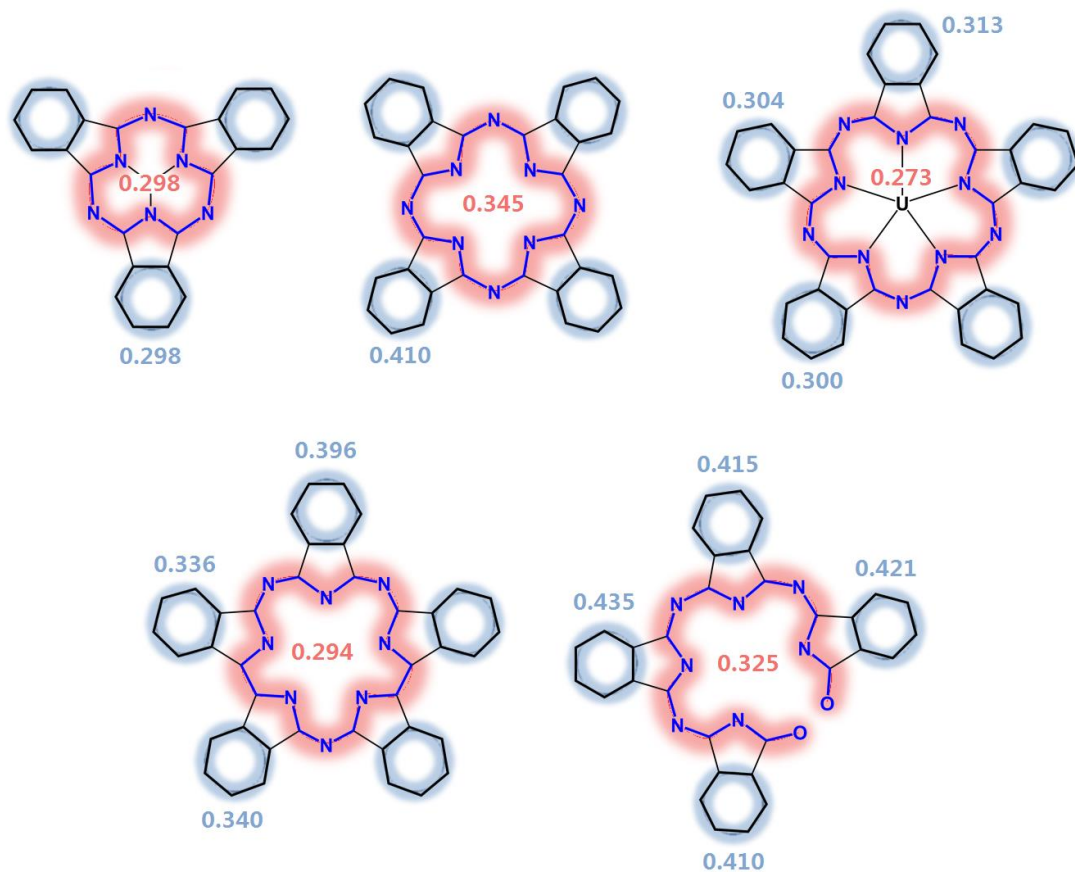


Fig. S23 The average π bond orders of the linear and cyclic conjugated routes in traditional cyclic conjugated oligoisoindoles together with phthalocyanine ring-cleavage derivative.

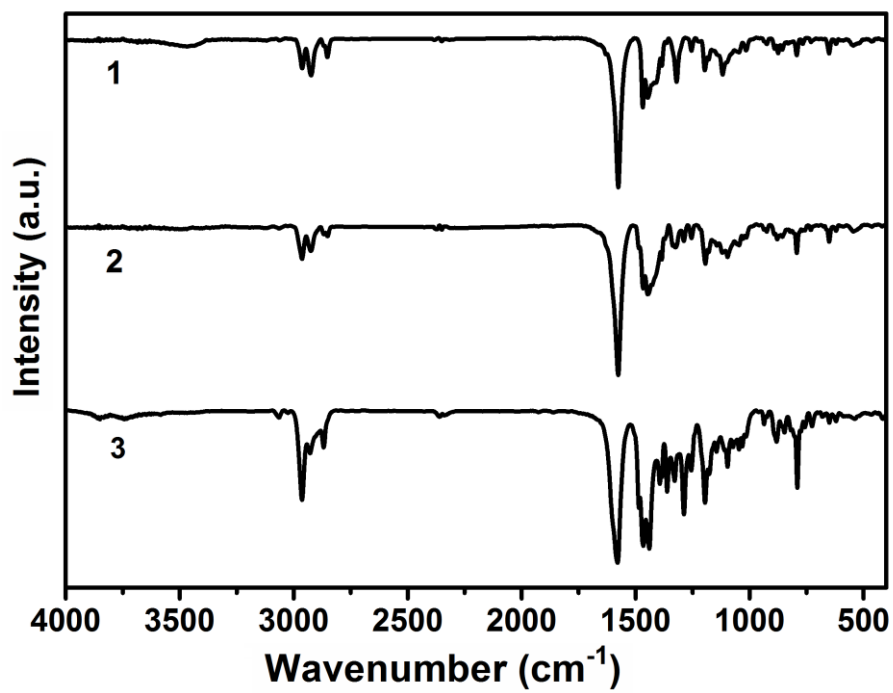


Fig. S24 IR spectra of **1-3** in the region of 400-4000 cm⁻¹.

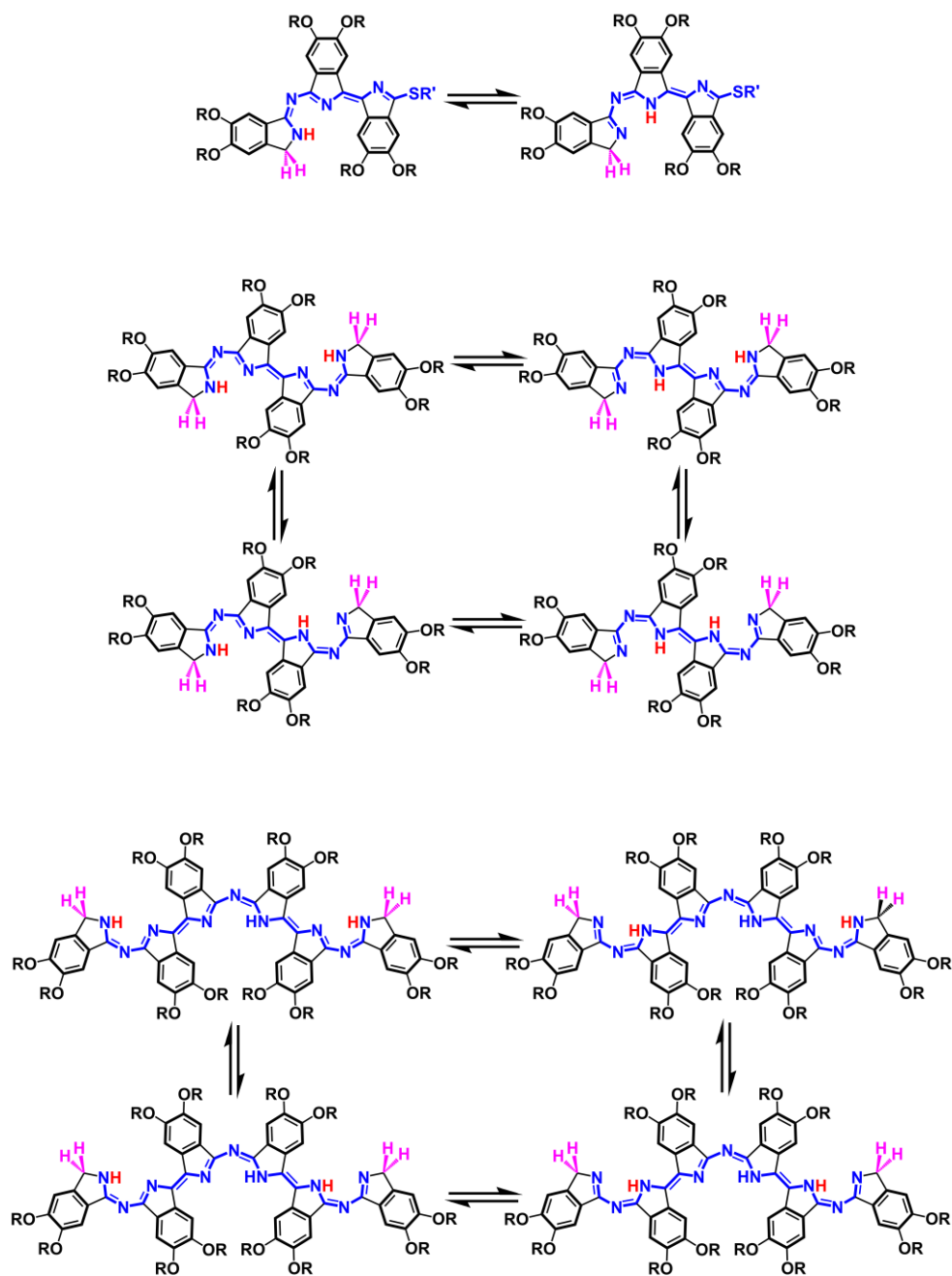


Fig. S25 The tautomeric conformations for compounds 2-4.

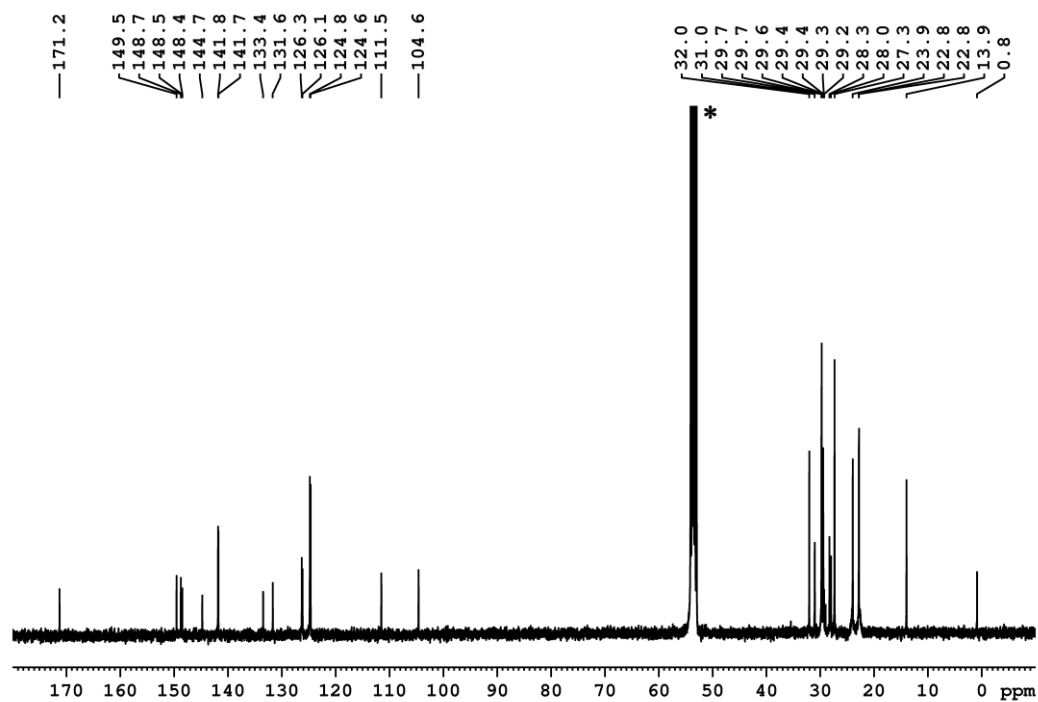


Fig. S26 ^{13}C NMR spectrum of compound **1** in CDCl_3 at 298K. * indicates the signals of residual solvent.

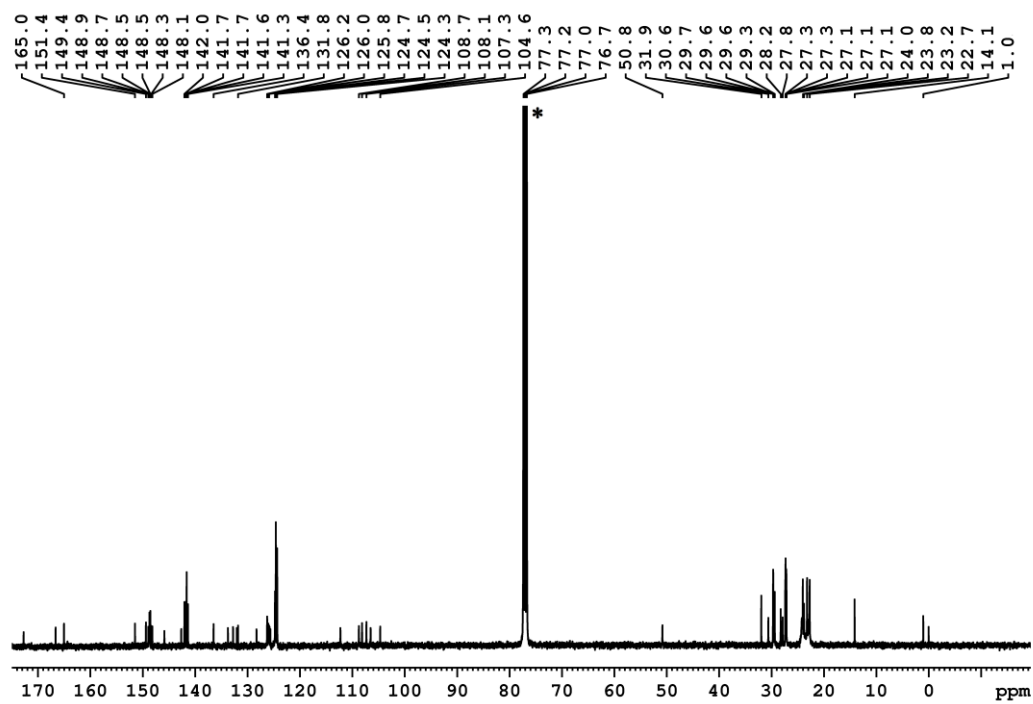


Fig. S27 ^{13}C NMR spectrum of compound **2** in CDCl_3 at 298K. * indicates the signals of residual solvent.

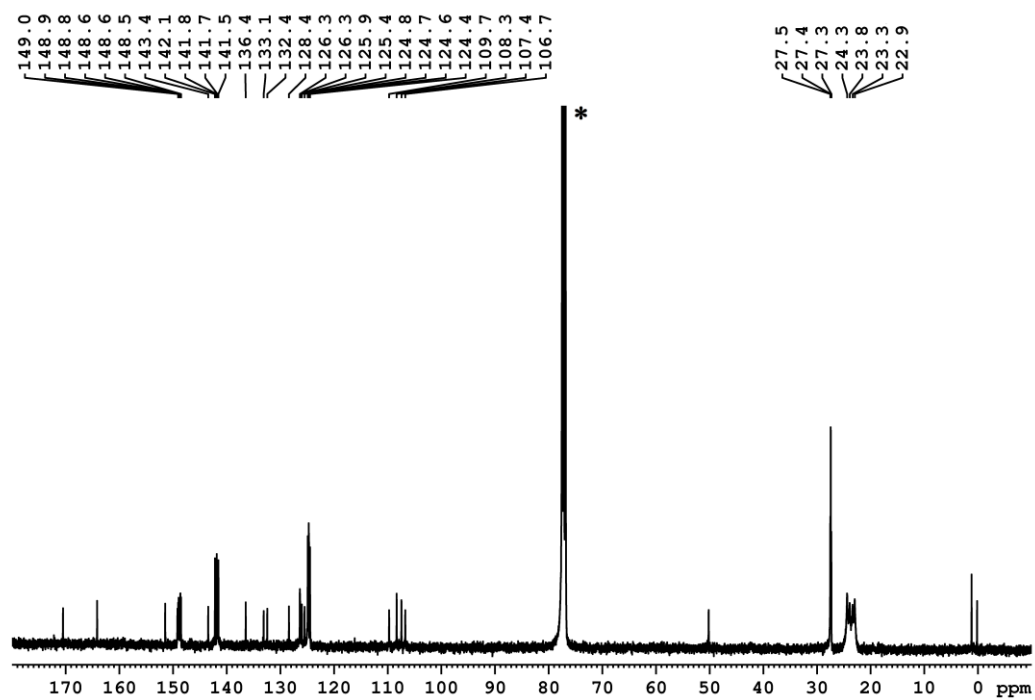


Fig. S28 ^{13}C NMR spectrum of compound **3** in CDCl_3 at 298K. * indicates the signals of residual solvent.

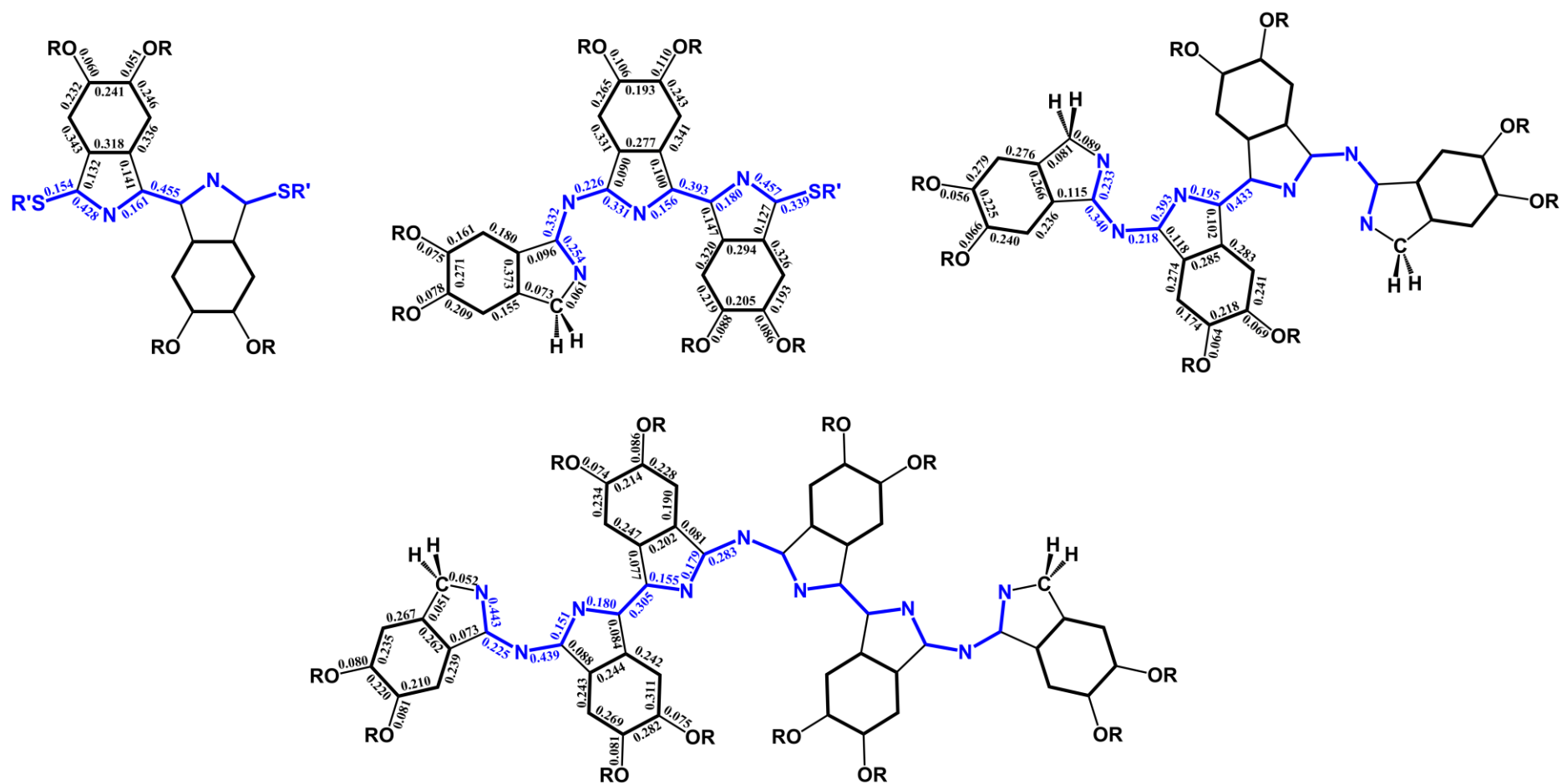


Fig. S29 The π MBO of 1-4.

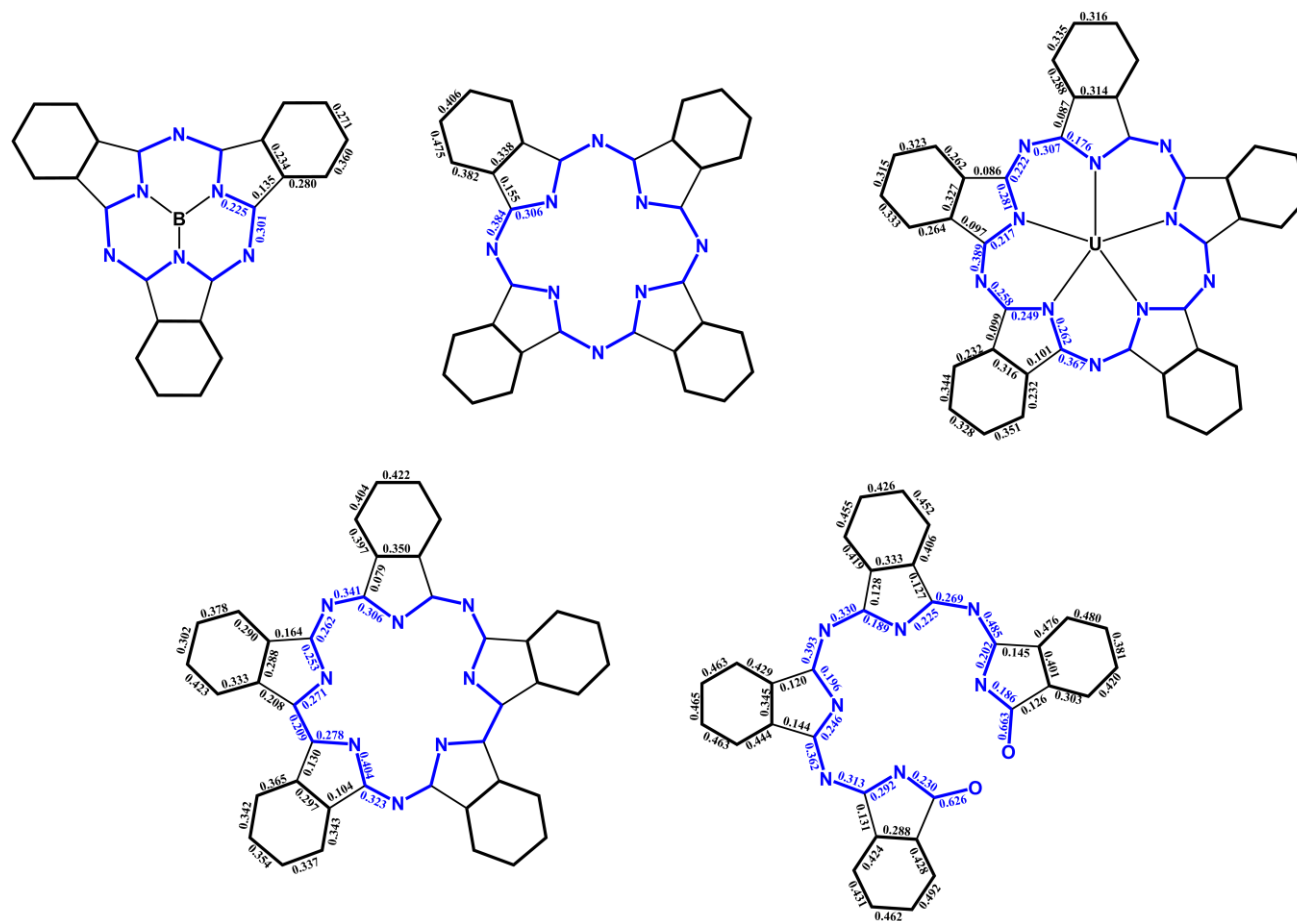


Fig. S30 The π MBO of the traditional cyclic conjugated oligoisoindoles together with the phthalocyanine ring-cleavage derivative.

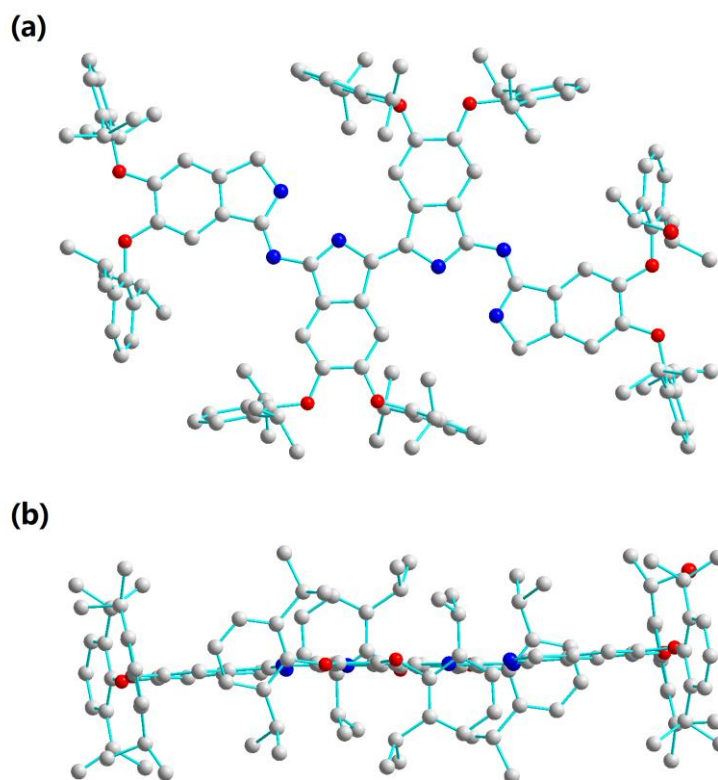
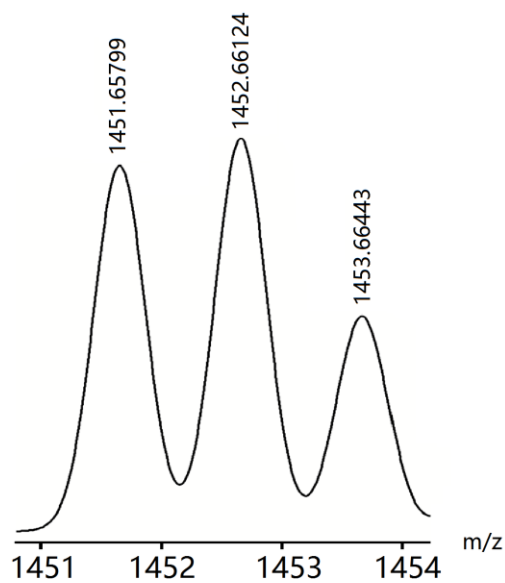
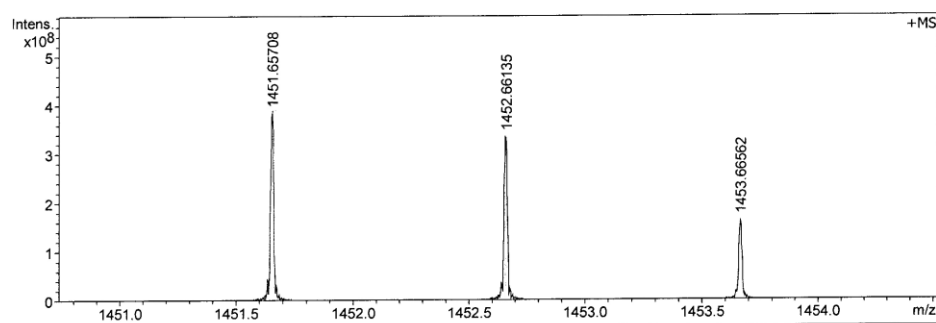


Fig. S31 Molecular structure of **3** in top view (a) and side view (b). Hydrogen atoms are omitted for clarity (C grey, N blue, O red).

(a)



(b)



(c)

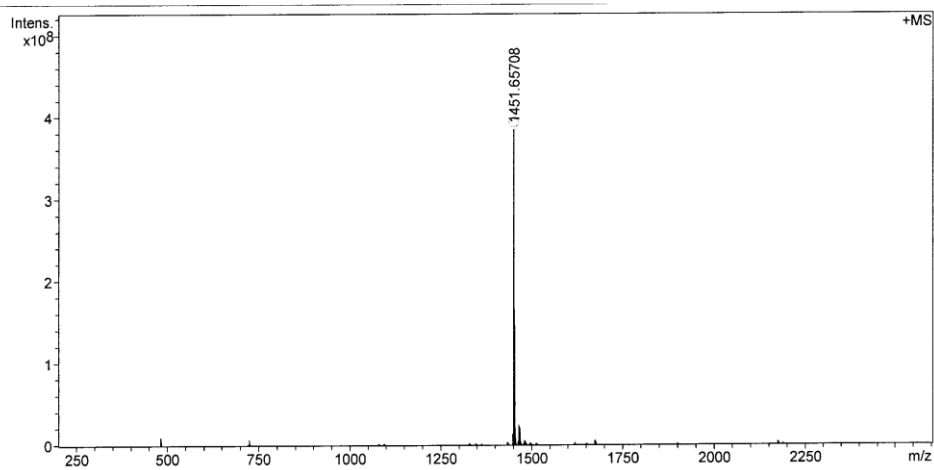


Fig. S32 Simulated (a) and experimental isotopic (b) pattern of $[M-H]^+$ and HR MS (c) for **5**.

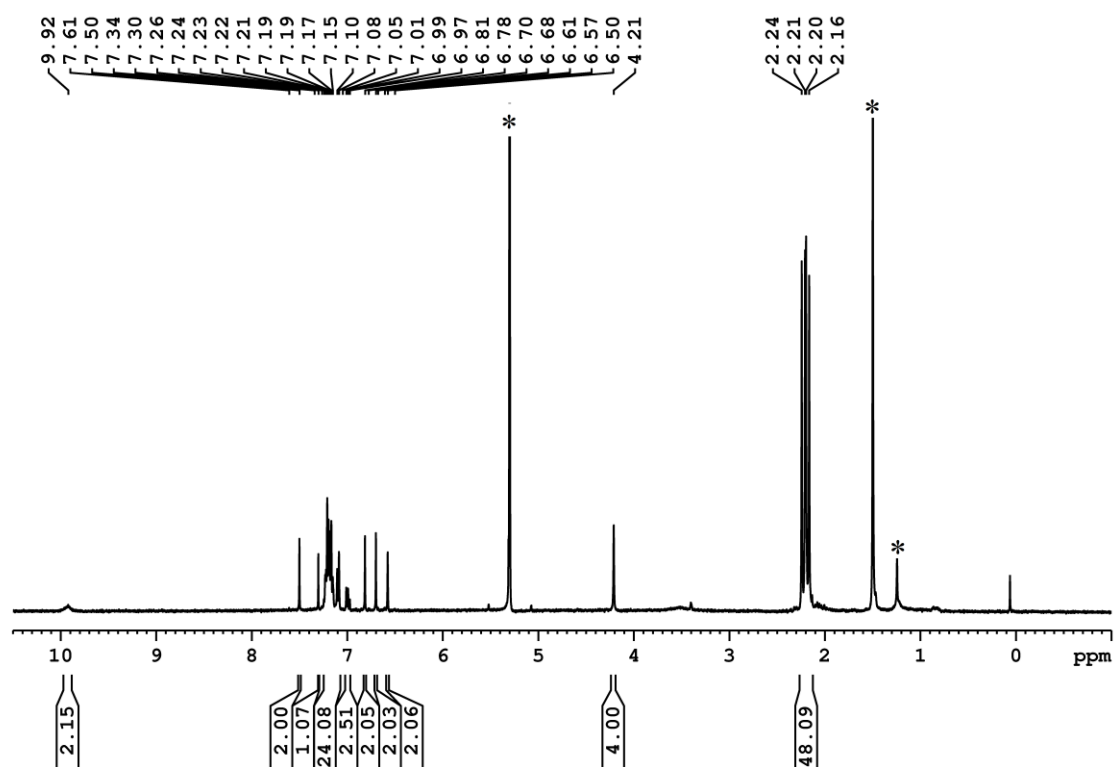


Fig. S33 ^1H NMR spectrum of **5** in CD_2Cl_2 at 298K; * indicates the signals for residual solvents.

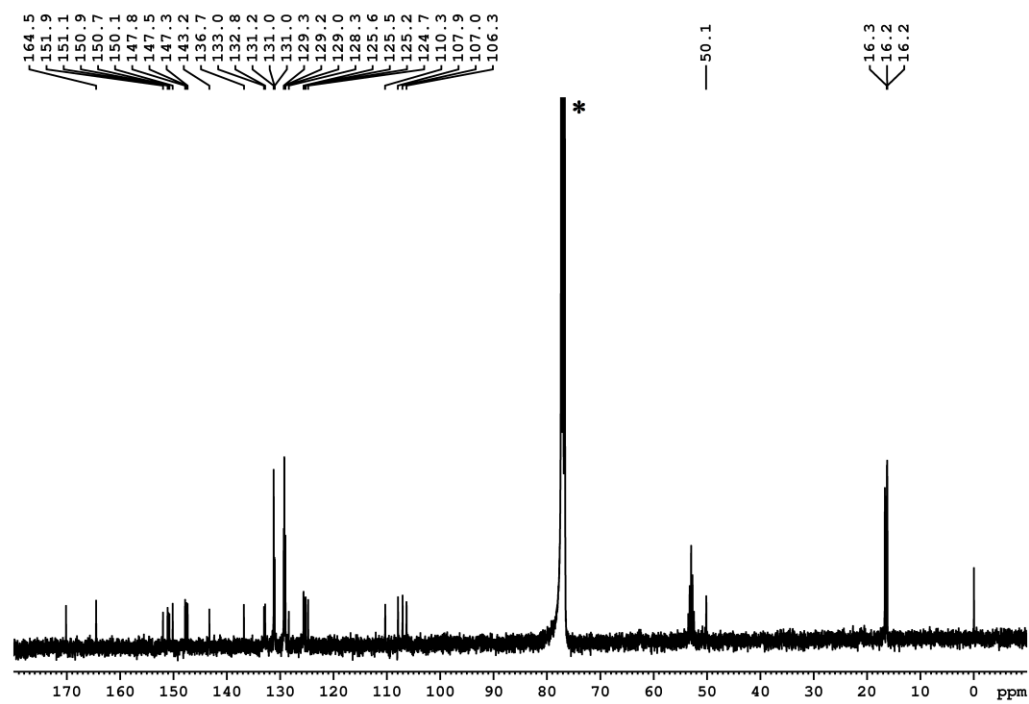


Fig. S34 ^{13}C NMR spectrum of **5** in CDCl_3 at 298K. * indicates the signals of residual solvent.

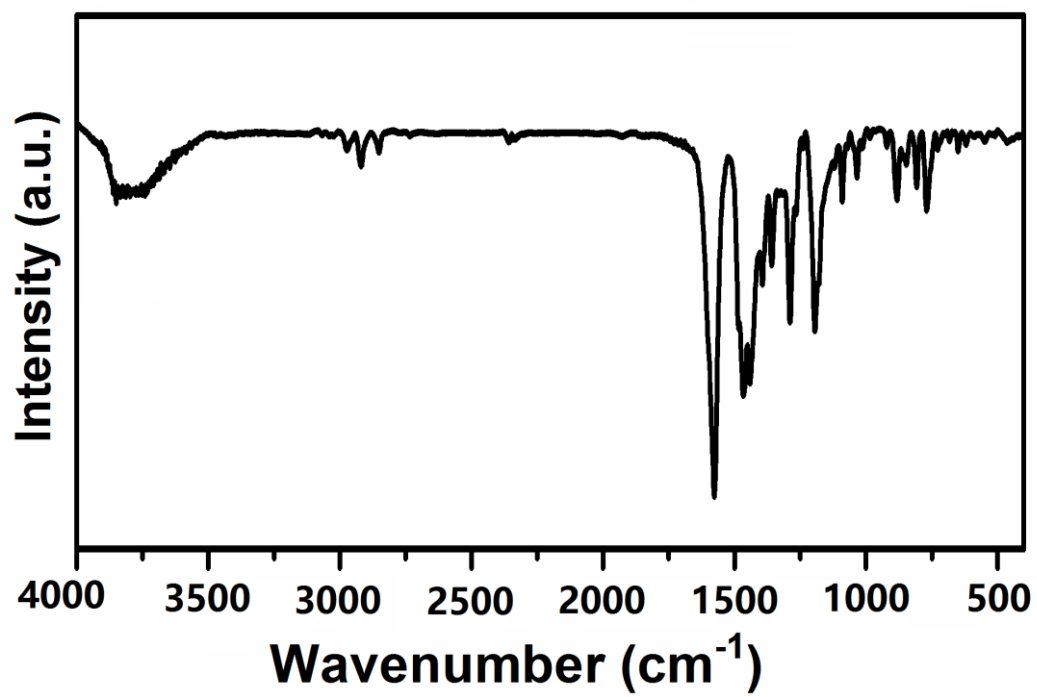


Fig. S35 IR spectrum of **5** in the region of 400-4000 cm⁻¹.

Table S1. ^1H NMR data (δ) for compounds **1-4** in CD_2Cl_2 at 298K.

Compound	H_{NH}	H_α	H_{aryl}	$\text{H}_{\text{methyne}}$	H_{methyl}	$\text{H}_{\text{SC12H25}}$	$\text{H}_{\text{terminal}}$
1	--	7.77 (s, 2 H), 6.42(s, 2 H)	7.27-7.23 (m, 12 H)	3.16-3.13 (m, 8 H)	1.25-1.06 (m, 88 H) ^a	2.81 (t, 4H, $J=4\text{Hz}$), 1.25-1.06 (m, 88 H), ^a 0.86 (t, 6H, $J=4\text{Hz}$)	--
2	9.84 (br, 1H)	7.92 (s, 1 H), 6.85 (s, 1 H), 6.67 (s, 1H), 6.59 (s, 1H), 6.44 (s, 1 H), 7.40-7.22 (m, 19 H) ^a	7.41-7.23 (m, 19 H) ^a	3.16-3.10 (m, 12 H)	1.25-1.07 (m, 92 H) ^a	2.70 (t, 2H, $J=4\text{Hz}$), 1.25-1.07 (m, 92 H), ^a 0.85 (t, 3H, $J=4\text{Hz}$)	4.05 (s, 2H)
3	9.69 (br, 2 H)	7.52 (s, 2 H), 6.83(s, 2 H), 6.70 (s, 2 H), 6.56 (s, 2 H) 7.52 (s, 2 H)	7.37-7.08 (m, 24 H)	3.19-3.12 (m, 16 H)	1.12-1.06 (m, 96 H)	--	3.96 (s, 4 H)
4	10.02 (br, 2 H) 8.85 (br, 1 H)	6.92 (m, 4 H) ^a 6.74 (s, 2 H) 6.62-6.57 (m, 6 H) ^a 6.31 (m, 4 H) ^a	7.42-7.19 (m, 30 H) 6.92 (m, 4 H) ^a 6.62-6.57 (m, 6 H) ^a 6.31 (m, 4 H) ^a	3.47-2.98 (m, 24 H)	1.33-0.72 (m, 144 H)	--	4.17 (s, 4 H)

^a These protons are overlapped.

Table S2. Crystallographic data for **1**, **3**, **4**, and **5**.

Compound	1	3	4	5
Molecular formula	C ₈₈ H ₁₂₂ N ₂ O ₄ S ₂	C ₁₃₂ H ₁₅₄ Cl ₁₂ N ₆ O ₈	C ₂₀₂ H ₂₄₉ Cl ₁₄ N ₉ O ₁₅	C ₁₀₀ H ₉₆ Cl ₆ N ₆ O ₁₀
<i>M</i>	1336.00	2378.01	3439.40	1754.53
Crystal system	triclinic	monoclinic	triclinic	Triclinic
Space group	<i>P1</i>	<i>P21/c</i>	<i>P-1</i>	<i>P-1</i>
<i>a</i> /Å	8.9041(4)	9.9153(2)	18.0089(5)	9.8074(5)
<i>b</i> /Å	14.0916(7)	27.3670(5)	19.4187(5)	13.2321(5)
<i>c</i> /Å	16.2768(8)	23.7531(4)	29.7417(7)	17.7176(7)
α /°	104.121(4)	90	90.357(2)	100.836(3)
β /°	91.824(4)	93.290(2)	95.539(2)	99.601(4)
γ /°	94.954(4)	90	107.328(2)	93.264(3)
<i>U</i> /Å ³	1970.23(16)	6434.8(2)	9875.8(4)	2217.35(17)
<i>Z</i>	1	2	2	1
<i>D_c</i> /Mg m ⁻³	1.126	1.227	1.190	1.314
μ /mm ⁻¹	0.989	2.807	2.264	2.281
Data collection range/°	3.25 to 67.14	3.23 to 65.00	3.22 to 67.27	3.41 to 66.99
Reflections collected / unique	24257 / 12106 [R(int) = 0.0380]	21859 / 10891 [R(int) = 0.0226]	67519 / 34508 [R(int) = 0.0394]	14923 / 7686 [R(int) = 0.0199]
Data/restraints/parameters	12106 / 3 / 883	10891 / 0 / 741	34508 / 19 / 2215	7686 / 0 / 560
<i>R</i> ₁ [<i>I</i> > 2σ(<i>I</i>)]	0.0466	0.0802	0.1121	0.0658
<i>wR</i> ₂ [<i>I</i> > 2σ(<i>I</i>)]	0.1245	0.2411	0.3263	0.1830
Goodness of fit	1.024	1.063	1.300	1.018

Table S3. Electron density difference plots of electron transitions (isovalue: $2.0 \times 10^{-4} e au^{-3}$) for **1**. Electron densities move from the cyan area to the purple area. Excited states with less than 30000 cm^{-1} and configurations which contribute more than 5% are shown (assignment: H = HOMO, L = LUMO, L+1 = LUMO+1, H-1 = HOMO-1, etc.).

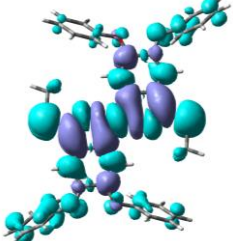
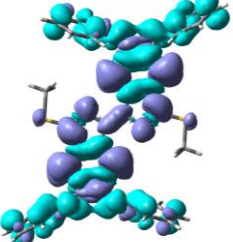
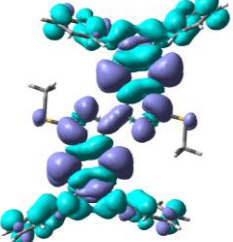
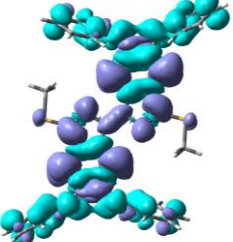
	<p>459.26 nm_3 Main Transitions: H→L(89%) H-4→L(8%)</p>		<p>387.05 nm_5 Main Transitions: H-4→L(89%) H→L(8%)</p>
	<p>292.18 nm_19 Main Transitions: H-2→L+1 (86%)</p>		<p>250.32 nm_40 Main Transitions: H-2→L+3(16%) H-2→L+7(28%) H-1→L+4(14%) H-1→L+8(31%)</p>

Table S4. Electron density difference plots of electron transitions (isovalue: $2.0 \times 10^{-4} e a.u.^{-3}$) for **2**. Electron densities move from the cyan area to the purple area. Excited states with less than 30000 cm^{-1} and configurations which contribute more than 5% are shown (assignment: H = HOMO, L = LUMO, L+1 = LUMO+1, H-1 = HOMO-1, etc.).

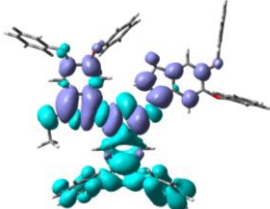
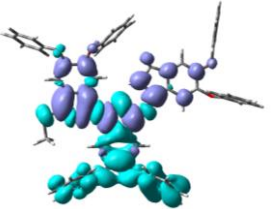
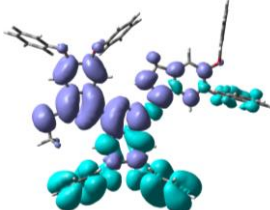
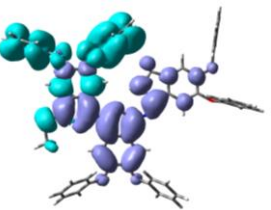
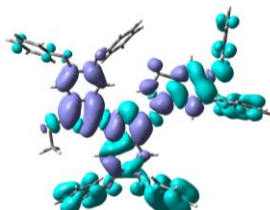
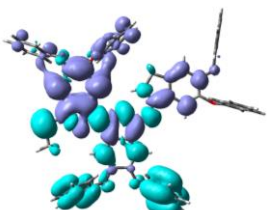
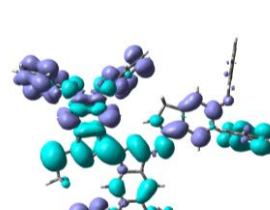
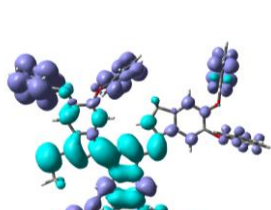
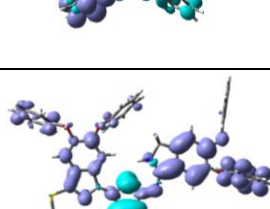
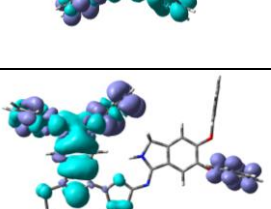
	512.01 nm_1 Main Transitions: H-1→L(47%) H→L(50%)		493.26 nm_2 Main Transitions: H-1→L(52%) H→L(45%)
	417.01 nm_4 Main Transitions: H-3→L (97%)		388.28 nm_6 Main Transitions: H-5→L(94%)
	352.52 nm_9 Main Transitions: H-7→L(36%) H-6→L(34%) H→L+1(20%)		337.74 nm_12 Main Transitions: H-9→L(33%) H→L+2(52%)
	285.32 nm_36 Main Transitions: H-4→L+1(10%) H-3→L+1(6%) H-2→L+2(25%) H→L+8(7%) H→L+9(34%)		283.12 nm_39 Main Transitions: H-1→L+4(27%) H→L+8(29%) H→L+9(19%)
	247.82 nm_77 Main Transitions: H-9→L+1(25%) H-1→L+14(46%)		247.15 nm_78 Main Transitions: H-2→L+9(43%) H-1→L+11(52%)

Table S5. Electron density difference plots of electron transitions (isovalue: $2.0 \times 10^{-4} e au^{-3}$) for **3**. Electron densities move from the cyan area to the purple area. Excited states with less than 30000 cm^{-1} and configurations which contribute more than 5% are shown (assignment: H = HOMO, L = LUMO, L+1 = LUMO+1, H-1 = HOMO-1, etc.).

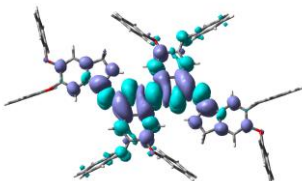
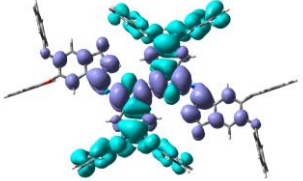
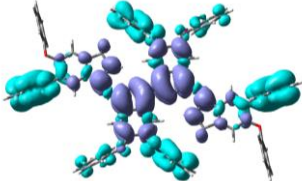
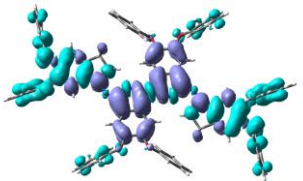
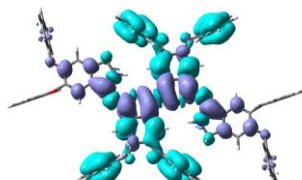
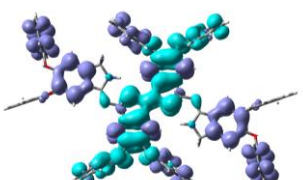
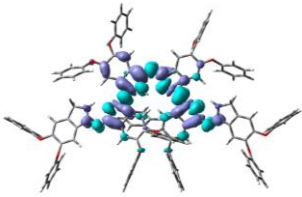
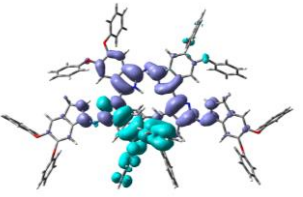
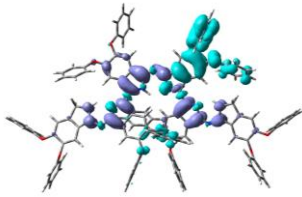
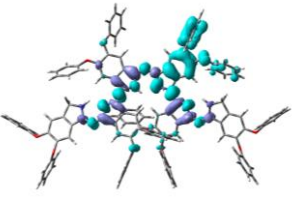
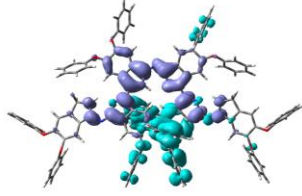
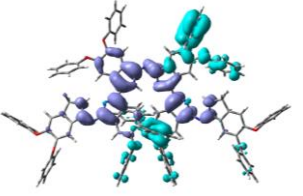
	544.99 nm_1 Main Transitions: H→L(96%)		474.86 nm_2 Main Transitions: H-1→L(96%)
	399.11 nm_5 Main Transitions: H-6→L (34%) H-4→L(64%)		350.95 nm_13 Main Transitions: H-8→L(68%) H→L+2(24%)
	331.76 nm_19 Main Transitions: H-11→L(77%) H→L+2(7%)		282.67 nm_55 Main Transitions: H-2→L+5(22%) H-1→L+4(26%) H-1→L+6(21%) H→L+18(10%)

Table S6. Electron density difference plots of electron transitions (isovalue: $2.0 \times 10^{-4} e au^{-3}$) for **4**. Electron densities move from the cyan area to the purple area. Excited states with less than 30000 cm^{-1} and configurations which contribute more than 5% are shown (assignment: H = HOMO, L = LUMO, L+1 = LUMO+1, H-1 = HOMO-1, etc.).

	744.97 nm_1 Main Transitions: H→L(99%)		496.37 nm_4 Main Transitions: H-3→L(86%) H→L+1(6%)
	493.34 nm_5 Main Transitions: H-4→L(60%) H-3→L(9%) H-1→L(11%) H→L+1(15%)		464.97 nm_6 Main Transitions: H-4→L(34%) H-1→L(22%) H→L+1(35%)
	446.86 nm_8 Main Transitions: H-6→L(91%)		424.92 nm_10 Main Transitions: H-8→L(26%) H-7→L(62%)